

The Diverse Properties of the Most Ultraviolet Luminous Galaxies Discovered by the *Galaxy Evolution Explorer*

Charles G. Hoopes¹, Timothy M. Heckman¹, Samir Salim², Mark Seibert³, Christy A. Tremonti⁴, David Schiminovich⁵, R. Michael Rich², D. Christopher Martin³, Stephane Charlot^{6,7}, Guinevere Kauffmann⁶, Karl Forster³, Peter G. Friedman³, Patrick Morrissey³, Susan G. Neff⁸, Todd Small³, Ted K. Wyder³, Luciana Bianchi¹, Jose Donas⁹, Young-Wook Lee¹⁰, Barry F. Madore¹¹, Bruno Milliard⁹, Alex S. Szalay¹, Barry Y. Welsh¹², Sukyoung K. Yi¹⁰

ABSTRACT

We report on the properties of a sample of ultraviolet luminous galaxies (UVLGs) selected by matching the *Galaxy Evolution Explorer* (*GALEX*) All-sky Imaging and Medium Imaging Surveys with the Sloan Digital Sky Survey Third Data Release. The overlap between these two surveys is roughly 450 square degrees. Out of 25362 galaxies (with SDSS spectroscopy) between $0.0 < z < 0.3$ detected by *GALEX*, there are 215 galaxies with $L > 2 \times 10^{10} L_{\odot}$ at 1530 Å (observed wavelength). The properties of this population are well correlated with ultraviolet surface brightness. We find that the galaxies with low UV surface brightness are primarily large spiral systems with a mixture of old and young stellar populations, while the high surface brightness galaxies consist primarily of compact starburst systems, with an approximate boundary at a surface brightness of $I_{1530} = 10^8 L_{\odot} \text{ kpc}^{-2}$. The large galaxies appear to be the high-luminosity tail of the galaxy star formation function, and owe their large luminosity to their large surface area. In terms of the behavior of surface brightness with luminosity, size with luminosity, the mass-metallicity relation, and other parameters, the compact UVLGs clearly depart from the trends established by the full sample of galaxies. The subset of compact UVLGs with the highest surface brightness ($I_{1530} > 10^9 L_{\odot} \text{ kpc}^{-2}$; “supercompact UVLGs”) have characteristics that are remarkably similar to Lyman Break Galaxies at higher redshift. They are much more luminous (and thus have much higher star formation rates) than typical local ultraviolet-bright starburst galaxies and blue compact dwarf galaxies. They have metallicities that are systematically lower than normal galaxies of the same stellar mass, indicating that they are less chemically evolved. In all these respects, they are the best local analogs for Lyman Break Galaxies.

¹Department of Physics and Astronomy, The Johns Hopkins University, Homewood Campus, Baltimore, MD 21218

²Department of Physics and Astronomy, University of California, Los Angeles, CA 90095

³California Institute of Technology, MC 405-47, 1200 East California Boulevard, Pasadena, CA 91125

⁴Steward Observatory, University of Arizona, 933 North Cherry Avenue, Tucson, AZ 85721

⁵Department of Astronomy, Columbia University, New York, NY 10027

⁶Max-Planck-Institut für Astrophysik, Karl-Schwarzschild-Str. 1, D-85748 Garching bei München, Germany

⁷Institut d’Astrophysique de Paris, UMR 7095, 98 bis Boulevard Arago, F-75014 Paris, France

⁸Laboratory for Astronomy and Solar Physics, NASA Goddard Space Flight Center, Greenbelt, MD 20771

⁹Laboratoire d’Astrophysique de Marseille, BP 8, Traverse du Siphon, 13376 Marseille Cedex 12, France

¹⁰Center for Space Astrophysics, Yonsei University, Seoul 120-749, Korea

¹¹Observatories of the Carnegie Institution of Washington, 813 Santa Barbara St., Pasadena, CA 91101

¹²Space Sciences Laboratory, University of California at Berkeley, 601 Campbell Hall, Berkeley, CA 94720

Subject headings: ultraviolet: galaxies – galaxies: starburst – galaxies: evolution

1. Introduction

Over the past decade enormous progress has been made toward mapping the cosmological history of star formation in the universe (*e.g.*, Madau et al. 1996; Giavalisco et al. 2004). This has mainly been accomplished using large samples of high-redshift galaxies selected by their rest-frame ultraviolet (UV) colors (*e.g.*, Steidel et al 1996, 2003; Dickinson et al. 2004). These surveys indicate that the global star formation rate of the universe has been in decline since $z \sim 1 - 2$, and was generally constant at higher redshift out to at least $z = 6$ (Giavalisco et al. 2004).

This picture still contains some uncertainty resulting from several factors. The star formation rate density at low redshift ($z = 0 - 1$) has been determined through different techniques (*e.g.*, H α luminosity) than those used for higher redshift galaxies (*e.g.*, rest-frame ultraviolet luminosity). These techniques are affected differently by extinction and radiative transfer effects, and they fundamentally probe star formation over different time scales.

One way around this problem is to obtain rest-frame ultraviolet (UV) measurements for a large sample of galaxies at low redshift, enabling the measurement of star formation rates using the same techniques that are used at higher redshift. This requires a UV telescope in space with a large field of view, something that has not been available until the *Galaxy Evolution Explorer (GALEX)* mission (Martin et al. 2005). *GALEX* is obtaining UV fluxes for more than $\sim 10^7$ galaxies in the redshift range of $0 < z < 2$. Initial results on the UV luminosity density show strong evolution from $z = 2$ to $z = 0$, with the strongest evolution occurring in the most UV luminous galaxies (Schiminovich et al. 2005; Arnouts et al. 2005). The fraction of galaxies with $L_{1530} > 0.2L_{*,z=3}$ fell by a factor of 30 from $z = 1$ to $z = 0$ (using $L_{*,z=3} = 6 \times 10^{10} L_{\odot}$; Steidel et al. 1999).

These UV luminous galaxies at high redshift are more commonly called Lyman Break Galaxies (LBGs; Steidel et al. 1999). These high-redshift galaxies are so named because they are identified by the effects of the Lyman break on their broadband colors (Steidel & Hamilton 1993). LBGs are UV bright galaxies undergoing intense star formation with low to moderate stellar masses ($\log M_* = 9.5$ to $11.0 M_{\odot}$), and are candidates for the precursors of present-day elliptical galaxies (see *e.g.*, Giavalisco 2002). LBGs are common at $z > 2$, and they are clearly important as the sites of a significant fraction of all the star formation in the universe. Since strong evolution has made objects like LBGs extremely rare in the local universe, all of the information on this important galaxy population has come from very distant samples, which are inherently difficult to study. Thus, there has been little detailed information available on the processes driving the evolution of star formation in the population of LBGs.

Using local UV-bright starbursts as local analogs to LBGs has contributed significantly toward understanding these objects (Heckman et al. 1998; Meurer et al. 1999). However, local starbursts differ from LBGs in important ways. Local starbursts are usually dwarf galaxies or small (sub-kpc) regions in the nuclei of larger galaxies, while LBGs have typical sizes of a few kpc (Ferguson et al. 2004). Luminous local starbursts are usually very dusty systems in which only a small fraction of the UV light escapes, while LBGs with similar bolometric luminosities (star formation rates) typically contain modest amounts of dust (*e.g.* Reddy et al. 2006; Erb et al. 2006b). Given these differences, it is not clear that the conditions in local starbursts or the triggers of star formation are identical to those in LBGs, and so there is a need for better LBG analogs in the local universe.

Since LBGs are found in part by their large UV luminosity, LBG analogs in the local universe should also be UV luminous. The large area UV sky surveys being carried out by *GALEX* provide an ideal data set for finding rare UV luminous galaxies in the local universe. Heckman et al. (2005; hereafter Paper I) described the properties of the most UV luminous galaxies (UVLGs) in the local universe based on cross-matching the initial *GALEX* surveys with the Sloan Digital Sky Survey (SDSS) first data release (DR1; Abazajian et al. 2003). The UVLGs were composed of two basic types of galaxies: Large UVLGs, which are characterized by lower UV surface brightness and high mass, and compact UVLGs, which have higher UV surface brightness and lower mass. Many of the compact UVLGs have properties very similar to LBGs.

Although this sample was very illuminating, several questions remain. The extent of the similarity between the compact UVLGs and LBGs is a crucial question. More generally, it is not known whether these galaxies are truly a distinct population of objects in an earlier phase of evolution, *i.e.*, remnants of the epoch of galaxy formation, or whether they are simply the high end of the UV luminosity function. Many of these questions could be better addressed if there were more such galaxies available for study, so we present an analysis of a larger sample of UVLGs, based on more recent *GALEX* and SDSS data.

2. Data

2.1. Ultraviolet Data

Since its launch in April, 2003, *GALEX* has been conducting several surveys of the UV sky. In this paper we make use of the *GALEX* All-sky Imaging Survey (AIS) and Medium-Deep Imaging Survey (MIS). The data were taken from the first public release of *GALEX* data (GR1) available at the Multimission Archive at Space Telescope (MAST). Details on the *GALEX* mission and surveys are given in Martin et al. (2005).

The *GALEX* data include far-ultraviolet (FUV; $\lambda_{eff} = 1528 \text{ \AA}$, $\Delta\lambda = 268 \text{ \AA}$) and near-ultraviolet (NUV; $\lambda_{eff} = 2271 \text{ \AA}$, $\Delta\lambda = 732 \text{ \AA}$) images with a circular field of view with radius $\sim 38'$. The spatial resolution is $\sim 5''$. Details of the *GALEX* satellite and data characteristics can be found in Morrissey et al. (2005).

The data were processed through the *GALEX* reduction pipeline at the California Institute of Technology. The pipeline reduces the data and automatically detects, measures, and produces catalogs of FUV and NUV fluxes for sources in the *GALEX* images.

2.2. Optical data

The *GALEX* catalogs were then matched to the SDSS Third Data Release (DR3; Abazajian et al. 2005) spectroscopic sample. The area of the overlap region between GR1 and DR3 is about 450 square degrees (Bianchi et al. 2006). The SDSS catalog provides (among many other available parameters) *ugriz* magnitudes, spectroscopic redshifts, concentration parameters, observed half-light radii and model-fit exponential scale lengths. To be included in our final matched catalog, we required that each source have a spectroscopic redshift in the range $0 < z < 0.3$, and that the SDSS source be spectroscopically classified as a galaxy, excluding objects classified by the SDSS pipeline as QSOs or Type I (broad line) AGN. The resulting GR1/DR3 sample contains 25362 galaxies. Of these, 18463 have 3σ FUV detections. The remaining galaxies were detected in the NUV images only.

With the distances estimated from the SDSS redshift, the FUV (and NUV) luminosity for each galaxy is known. Following Paper I, galaxies with $L_{1530} > 2 \times 10^{10} L_{\odot}$ qualify as UV luminous galaxies¹, where L_{1530} is the luminosity at the observed wavelength of 1530 Å. This luminosity is $\sim 5L_*$ for $z = 0$ (Wyder et al. 2005) and $\sim 0.3L_*$ for LBGs at $z = 3$ (Steidel et al. 1999). There are 235 galaxies in the GR1/DR3 sample that meet this criterion. We then inspected the SDSS spectra of these galaxies to eliminate broad line (Type I) AGN that were missed by the SDSS pipeline, as well as objects with BL Lac-type spectra (UV bright but with weak or non-existent emission lines). Type II AGN in the sample are discussed in section 4.4. The 215 galaxies that remain are hereafter referred to as ultraviolet luminous galaxies (UVLGs). These galaxies span the redshift range from $z = 0.053$ to $z = 0.3$.

A large number of galaxy parameters derived from the SDSS spectra are available in the value-added catalogs produced by the SDSS collaboration. These catalogs are available at the SDSS website at the Max Planck Institute (<http://www.mpa-garching.mpg.de/SDSS>). From these catalogs we use the emission line fluxes, widths, and derived metallicities. For more information on the derivation of these parameters, see Kauffmann et al. (2003a,b,c), Brinchmann et al. (2004), and Tremonti et al. (2004). These catalogs do not include metallicities for galaxies with an AGN contribution since this can strongly affect the line strengths, so only a subset of our sample have metallicity determinations. In addition, some galaxies have poor line flux measurements because the emission lines in the fiber aperture are weak or non-existent, *e.g.*, in galaxies with no star formation in the central region of the galaxy. Thus line flux measurements exist for only a subset of our sample.

2.3. Spectral Energy Distribution Modeling

To gain further information about the properties of the galaxies in our sample, we compared the observed optical and UV properties of our sample to a library of model spectral energy distributions (SEDs), following Salim et al. (2005). This was done by first constructing the broadband optical and UV SEDs from the SDSS and *GALEX* magnitudes. Each observed SED was then compared to an extensive library of SEDs generated by the Bruzual & Charlot (2003) population synthesis code. Each model galaxy is based on a star formation history composed of an exponentially declining star formation rate (SFR) with superimposed bursts of star formation, and includes the effects of attenuation by dust (see Charlot & Fall 2000). The library contains 10^5 models at each of five evenly spaced redshifts from $z = 0.05$ to $z = 0.25$, and the grid of models was constructed to span the likely range of star formation histories.

The goodness of fit for a given model to an observed SED is then translated to a probability that the parameters for that model apply to the galaxy. Thus the parameters of the best fitting model will have the highest probability, and a probability distribution can be constructed for the entire library at the appropriate redshift. From this the median and 95% confidence limits on each parameter can be determined. This was done for a list of parameters including stellar mass and star formation rate over a range of timescales. For more information on the SED fitting process, see Salim et al. (2005). In this paper the stellar masses and star formation rates were determined through SED fitting.

¹Throughout this paper we use $H_0 = 70 \text{ km s}^{-1}$, $\Omega_m = 0.3$, and $\Omega_{\Lambda} = 0.7$.

3. Properties of the GR1/DR3 Galaxy Sample

The *GALEX*-SDSS matched catalog provides a valuable resource for studying the UV-optical properties of star-forming galaxies in the local universe. In a future paper we will report on the analysis of the entire galaxy sample. Here we concentrate on the relationship between UVLGs and the broader galaxy population.

The galaxy sample considered here should be nearly devoid of unobscured (type I) AGN, so the dominant source of the UV light detected by *GALEX* is massive stars. The UV luminosity of a galaxy therefore traces the total amount of star formation in that galaxy over the past 10^8 years (Martin et al. 2005). We also have measurements of the sizes of these galaxies. Most of these galaxies are only marginally resolved in the *GALEX* images, so we used the half-light radii measured on the higher-resolution SDSS images. The SDSS *u*-band was chosen because it is the closest in wavelength to the *GALEX* bands and therefore the most likely to reflect the true spatial extent of star-formation. In most cases we use the scale length from the seeing-corrected exponential model fit calculated by the SDSS pipeline as the half-light radius. However, for well-resolved galaxies we found that the seeing-corrected radius derived from the exponential model fits is systematically *larger* than the directly observed half-light radius. We found that this occurs for galaxies with half-light radii larger than about $2.2''$. We thus use the observed *u*-band half-light radius as $r_{50,u}$ for galaxies larger than $2.2''$, and the seeing-corrected scale length as $r_{50,u}$ for galaxies smaller than $2.2''$. We can then calculate the effective surface brightness by dividing one-half of the luminosity by the area of the galaxy enclosed by the half-light radius ($I_{1530} = L_{1530}/2\pi r_{50,u}^2$).

Figure 1 shows a normalized contour plot of the FUV surface brightness versus FUV luminosity for the 18463 galaxies in the GR1/DR3 sample that were detected in the FUV images. The luminosity bins were normalized to have the same number of galaxies in each bin, thus clarifying the dependence of surface brightness on luminosity by removing the effects of having a smaller number of galaxies at the low and high luminosity ends of the distribution.

The plot shows a well-defined trend of slightly increasing surface brightness with increasing luminosity over the entire luminosity range. However, at the high luminosities corresponding to the UVLGs there is an anomalous population of galaxies that defy the general trend by having a much higher surface brightness than would be expected given their luminosity. These galaxies have $I_{1530} \geq 10^8 \text{ L}_\odot \text{ kpc}^{-2}$. Only among the UVLGs are galaxies with the highest surface brightnesses ($I_{1530} \geq 10^9 \text{ L}_\odot \text{ kpc}^{-2}$) relatively common.

Figure 2 shows the dependence of half-light radius on luminosity. The surface brightness parameter shown in Figure 1 depends on the half-light radius, so Figure 2 is an alternative representation of Figure 1. Over most of the range in luminosity the radius increases with increasing luminosity. Above $L_{1530} > 10^{10} \text{ L}_\odot$ there is a group of galaxies that do not obey this trend in the sense that they are too small for their luminosity. The dashed lines in Figure 2 are lines of constant I_{1530} , and the galaxies responsible for this deviation from the trend have $I_{1530} > 10^9 \text{ L}_\odot \text{ kpc}^{-2}$.

These two figures show that in general galaxies with higher UV luminosity are larger and have somewhat higher surface brightness than their less luminous counterparts. At high luminosities, however, some galaxies behave differently. They have small radii, but this is more than compensated by their increased surface brightness to put them among the most UV luminous galaxies in the sample. This is a strong indication that these UVLGs are distinct from the general galaxy population. By contrast, UVLGs with lower surface brightness do not distinguish themselves from the full sample of galaxies except by their luminosity. They appear to be the largest and therefore most luminous normal galaxies.

Figure 3 shows how the UV surface brightness changes with stellar mass, as determined from the SED

model fitting (Salim et al. 2005). In general the stellar mass determined in this manner agrees to within a factor of 2 with the dynamical mass calculated as $M_{dyn} = 3.4\sigma_{gas}^2 r_{50,u}/G$, where σ_{gas} is the standard deviation of the gas velocity measured from the emission lines. The coefficient 3.4 was taken from Erb et al. (2006) and represents a realistic estimate of the mass distribution for LBGs. The UV surface brightness is relatively constant over a wide range of stellar masses, and then slowly falls above a mass of $10^{10.5} M_{\odot}$. This implies that the more massive galaxies have correspondingly larger sizes over which the young stellar population is distributed. The drop in surface brightness above $10^{10.5} M_{\odot}$ may be related to the relatively abrupt transition in the galaxy population at this mass-scale between young disk-dominated galaxies and old bulge-dominated ones (e.g. Kauffmann et al. 2003b).

The points shown in Figure 3 are the locations of individual UVLGs. Unlike the galaxy population as-a-whole, the UVLGs show a clear inverse correlation between surface brightness and mass. We have already pointed out that this fact indicates that the more massive UVLGs owe their large luminosities to their large mass. The less massive UVLGs have high UV surface brightnesses indicative of intense star-formation. Figure 3 shows how the UVLGs relate to the rest of the sample in terms of mass (but keep in mind that the contours are normalized by the number of galaxies in each mass bin). The UVLGs with $I_{1530} < 10^8 L_{\odot} \text{ kpc}^{-2}$ are among the most massive star-forming galaxies in the GR1/DR3 sample, with $\log M_{*} \geq 10.5 M_{\odot}$. While these are the lower surface brightness component of the UVLG sample, they are still somewhat offset toward higher surface brightness than the full sample (they are not low surface brightness galaxies). In the main, their properties appear to be similar to those of large, disk galaxies (they are the extrema of the population).

The UVLGs with $I_{1530} > 10^8 L_{\odot} \text{ kpc}^{-2}$ are generally lower mass systems ($\log M_{*} \leq 10.5 M_{\odot}$). They clearly stand out from the full sample by having much higher surface brightness than would be expected for normal galaxies of similar mass. This is even more obvious for galaxies with $I_{1530} > 10^9 L_{\odot} \text{ kpc}^{-2}$, which would qualify as LBGs based on their FUV surface brightness.

Based on the analysis above, the UVLG population can be thought of as two very different types of galaxies. The high-surface brightness systems (“compact UVLGs”) have high star formation rates per unit area and would be called starburst galaxies, while the low surface brightness systems (“large UVLGs”) are large spirals, with high rates of total star formation but low rates of star formation per unit area. There is no clear transition from one population to the other, but a surface brightness value of $I_{1530} = 10^8 L_{\odot} \text{ kpc}^{-2}$ serves as a useful boundary. There are intermediate cases that do not fit cleanly into either category. Figure 3 shows that this surface brightness boundary corresponds to a stellar mass of roughly $M_{*} = 10^{10.5} M_{\odot}$ (similar to the mass scale that divides the bimodal galaxy population as-a-whole – e.g. Kauffmann et al. 2003b). Using this criterion there are 110 large UVLGs and 105 compact UVLGs in the GR1/DR3 sample. These two diverse populations were recognized in Paper I, but we can now place them firmly in the context of the overall galaxy population.

Throughout the rest of this paper we will distinguish between large and compact UVLGs. Note, however, that while the compact UVLGs have the properties of intense starbursts, not all of them have FUV surface brightnesses high enough to be considered typical LBGs, which generally have $I_{1530} > 10^9 L_{\odot} \text{ kpc}^{-2}$. We will consider the compact UVLGs that meet this more stringent surface brightness criterion as possible LBG analogs, and will refer to them as “supercompact UVLGs”. The GR1/DR3 sample contains 35 supercompact UVLGs.

4. Properties of Ultraviolet Luminous Galaxies

Since the UVLG sample was chosen based on an ultraviolet luminosity criterion, they are all expected to have high star formation rates. As in Paper I, the majority of UVLGs (83%) have concentration parameters $C < 2.6$, where C is defined as R_{90}/R_{50} , the ratio of the radius containing 90% of the Petrosian r -band luminosity to that containing 50%. These low concentration parameters are indicative of disk systems, as expected for a sample of star-forming galaxies. Yet as was made clear in the previous section, UVLGs span a wide range of properties. In this section we explore the properties of UVLGs. The properties of the 215 UVLGs are listed in Table 1.

4.1. Ultraviolet Surface Brightness

Figure 4 plots the FUV surface brightness of the 215 UVLGs against the FUV luminosity. The galaxies were chosen to be luminous, but they span a wide range in surface brightness, and there is no correlation between luminosity and surface brightness. This implies that the UVLGs span a similarly large range of size. This is confirmed in Figure 5, which plots the luminosity against the half-light radius. UVLGs range in half-light radius from less than a kpc to > 20 kpc. The dotted lines in Figure 5 show a constant surface brightness of $10^8 L_{\odot} \text{ kpc}^{-2}$ and $10^9 L_{\odot} \text{ kpc}^{-2}$, the latter being the lower limit seen in LBGs at $z = 3$ (Giavalisco 2002). Only a fraction of the UVLGs have surface brightnesses that rival those of LBGs, even though they all have LBG-like luminosities.

The FUV surface brightness is related to the star formation intensity, *i.e.*, the star formation rate per unit area. Figures 4 and 5 show then that only a subset of the UVLGs are luminous because they have high star formation intensities. The rest owe their high luminosities to their large size, *i.e.*, they have modest levels of star formation intensity spread over a large area.

This is also apparent in Figure 3, which shows more clearly the correlation between surface brightness and stellar mass noted above. The UVLGs with low surface brightness are the most massive, while the high surface brightness UVLGs are low-mass systems. The typical mass and surface brightness range of LBGs is shown in the figure (Shapley et al. 2001; Papovich et al. 2001; Giavalisco 2002). Figures 3 – 5 illustrate the fact that UVLGs span a continuous range of properties, *i.e.*, there is no clear demarcation between the large and compact samples. The division of the samples at a surface brightness of $I_{1530} > 10^8 L_{\odot} \text{ kpc}^{-2}$ is an arbitrary boundary.

4.2. Star Formation and Attenuation by Dust

Figure 6 shows the FUV- r color and NUV- r color for the 215 UVLGs as a function of surface brightness. Both colors are well-correlated with surface brightness, with the brightest galaxies having the bluest color. This agrees with the idea that the UV-optical colors are sensitive to the ratio of current to past star formation. Salim et al. (2005) showed the NUV- r in particular is a good tracer of the star formation rate parameter b , which is the current SFR divided by the past-average SFR. The blue color of the high surface brightness UVLGs can be understood if they are undergoing intense starbursts which are much more significant than the past average rate of star formation. The FUV surface brightness appears to be a good indicator of star formation intensity for UV-selected galaxies. The typical colors of LBGs are also indicated in the plot (Shapley et al. 2001; Papovich et al. 2001; Giavalisco 2002).

Figure 7 shows the FUV surface brightness versus the specific star formation rate (star formation rate normalized by stellar mass). The extinction-corrected star formation rates were determined by SED model fitting. We have also calculated star formation rates using the H α luminosity in the SDSS spectra using the recipe given in Kennicutt (1998), these values generally agree within a factor of 2, which is quite good considering that the H-alpha measurements were taken through 3'' fibers. The specific star formation rate relates the current to past star formation, and the inverse of this quantity is the “galaxy building time,” the time it would take to build up the current stellar mass at the current SFR. The specific star formation rate is clearly correlated with the FUV surface brightness, with the high surface brightness systems generally have the highest specific SFRs and short building times, indicating that these are starburst systems. The large UVLGs have galaxy building times of roughly a Hubble time, as expected for a galaxy that has been built up over the age of the universe at a constant or slowly varying rate of star formation. Galaxy building times of less than 1 Gyr are typical for LBGs (Shapley et al. 2001; Papovich et al. 2001; Giavalisco 2002), and the high surface brightness UVLGs overlap this range. However some of the high surface brightness systems have lower specific SFRs and longer building times than typical LBGs, which suggests that they have had significant star formation prior to the current burst. *Spitzer* imaging of LBGs indicates that they do not have significant populations of older stars (Barmby et al. 2004), suggesting that LBGs are undergoing their first major burst of star formation. If this is the case, then these systems with longer building times may not be true analogs for LBGs. However, there is a significant fraction of the high-surface brightness systems that fall in the boundaries set by the LBGs, and these may be excellent analogs.

Figure 8 shows the FUV attenuation as a function of surface brightness. The FUV attenuation was determined using the Balmer decrement and the Calzetti (2001) starburst attenuation law. The compact UVLGs are in the range $A_{1530} \leq 2$, indicating that a relatively large fraction ($> 10\%$) of the UV light escapes. The large UVLGs are mostly in the range from 0 to > 4 magnitudes of attenuation. Figure 8 shows that compact UVLGs have a lower amount of attenuation on average than do large UVLGs, and the higher surface brightness compact UVLGs have still lower average extinction values. We note that this method of determining attenuation values uses the SDSS fiber spectra and may be sensitive to aperture effects. The fibers capture most of the light from the compact UVLGs, so this should only be an issue for the large UVLGs, where we are measuring the attenuation in the central core of the galaxy. Figure 8 also shows the typical range of FUV attenuation seen in LBGs (Shapley et al. 2001; Papovich et al. 2001).

4.3. Metallicity

Figure 9 shows two determinations of the mass *vs.* metallicity relation for the entire GR1/DR3 sample. The left panel shows the relation determined via the method of Tremonti et al. (2004). This method makes use of a grid of models, which combine the Bruzual & Charlot (2003) population synthesis code with photo-ionization models of H II regions. The methodology is described in detail in Charlot & Longhetti (2001). Metallicities are constrained by fitting all the strong emission lines in the SDSS spectra. Only 129 of the UVLGs have metallicity determinations from the SDSS spectra, because galaxies with an AGN contribution to their spectra were excluded. The well-known mass-metallicity relation (Tremonti et al. 2004) is apparent in Figure 9, and the best fit to the Tremonti et al. sample is shown as a dotted line. The UVLGs also show a relation between mass and metallicity, but it is offset from the general sample. At high masses ($> 10^{10.5} M_{\odot}$) most of the UVLGs have metallicities similar to those of normal galaxies. Most of these objects are the large UVLGs, which we have argued are just the UV-bright tail of the population of normal high-mass star forming galaxies. Their relatively normal metallicities support this idea. At lower masses (where the sample

is primarily the compact UVLGs), the slope of the mass-metallicity relation for the UVLGs is significantly steeper than that of the overall galaxy population. In the mass range $\sim 10^9$ to $10^{10} M_{\odot}$, the compact UVLGs have metallicities a factor of two to three lower than normal galaxies of the same mass.

Selection on the basis of high UV luminosity could clearly bias the sample against dusty objects, and the dust/gas ratio will be larger for higher metallicity. Thus, selection effects could make a UV-bright sample have systematically lower metallicity. While such an effect may be present, it does not explain the mass-dependence of the offset between the mass-metallicity relation for the sample as-a-whole, and that of the UVLGs.

It is very interesting to compare the mass-metallicity relation for the UVLGs to what is found for UV-bright galaxies at higher redshifts. The form of the mass-metallicity relation for the UVLGs is similar to that found by Savaglio et al. (2005), who investigated a sample of star-forming galaxies at $z = 0.7$. Their relation is shown in the left panel of Figure 9. They interpreted the change in the form of the mass-metallicity relation from $z \sim 0.1$ to ~ 0.7 in terms of the “down-sizing” of the galaxy population. Massive galaxies have essentially the same metallicity at $z \sim 0.1$ and ~ 0.7 because this population has already come near the end-point of its evolution by $z \sim 0.7$. The strong chemical evolution at late times seen in the low mass galaxies is because they are still converting significant mass from gas into stars at the present time. Applied to the compact UVLGs, this would suggest that they are relatively unevolved compared to typical galaxies of the same mass. Alternatively, perhaps the compact UVLGs are UV-bright because they are experiencing a burst of star formation triggered by the infall of metal-poor gas.

Erb et al. (2006) have measured the mass-metallicity relation for LBGs at $z \sim 2$. They find that this relation has evolved considerably compared to the local universe, with LBGs having systematically lower metallicities than present-day galaxies by a factor of about two *for all masses*. Erb et al. estimate metallicity using the $N2$ method, which uses the $[N II]/H\alpha$ ratio, as calibrated by Pettini & Pagel (2004). The resulting metallicities are known to be systematically lower than those obtained using the Tremonti et al. (2004) method. To fairly compare the UVLGs and LBGs, we also plot our mass-metallicity relation based on the Pettini & Pagel (2004) method (right panel of Figure 9). While the shape of the relation changes, the offset of the compact UVLGs from the rest of the galaxy population at low mass remains. The dashed line shows the relation for LBGs from Erb et al. (2006). At low masses ($< 10^{10.5} M_{\odot}$) the compact UVLGs and LBGs have similar metallicity. At higher masses the UVLGs are more metal-rich (including the compact UVLGs). Erb et al. interpret the relation for the LBGs in terms of the loss of metals by supernova-driven winds that is occurring at all masses. Results by Shapley et al. (2005) suggest this may also be true at redshifts as low as 1 to 1.5 (Shapley et al. 2005). This contrasts with the mass-dependent loss of metals inferred for the local galaxy population (Tremonti et al. 2004). The form of the mass-metallicity relation for the UVLGs suggests mass-dependent metal loss. We will consider this idea in detail in a future paper.

Figure 10 shows the metallicity of the ionized gas, determined from the SDSS spectra (Tremonti et al. 2004), in UVLGs as a function of FUV surface brightness. There is a clear trend of increasing metallicity with decreasing surface brightness. Given the connection between surface brightness and mass previously discussed (see Figure 3), this is likely a reflection of the mass-metallicity correlation. The high surface brightness galaxies have the lowest metallicity, and this metallicity is typical of that found in LBGs (Shapley et al. 2004; Erb et al. 2006).

4.4. Active Galactic Nuclei

Figure 11 is a diagnostic diagram that uses line ratios to differentiate between active galactic nuclei (AGN) and star-formation-dominated systems (Baldwin et al. 1981). The dashed line in the figure shows the line of demarcation determined by Kauffmann et al. (2003a) for SDSS galaxies, where galaxies below the line are dominated by star formation. The UVLGs are shown in the figure as large circles, with filled circles denoting UVLGs with $I_{1530} > 10^8 \text{ L}_\odot \text{ kpc}^{-2}$ and crosses denoting UVLGs with $I_{1530} > 10^9 \text{ L}_\odot \text{ kpc}^{-2}$. Of the 104 compact (and supercompact) UVLGs in this plot, 22 are classified as AGN or transition objects, roughly 21%, compared to 33% of the entire sample in the compact UVLG mass range ($9.0 \text{ M}_\odot \leq \log M_* \leq 11.0 \text{ M}_\odot$). About 34% of the large UVLGs in this diagram ($I_{1530} < 10^8 \text{ L}_\odot \text{ kpc}^{-2}$) are classified as AGN (36 out of 106), while for the entire sample in this mass range ($10.3 \text{ M}_\odot \leq \log M_* \leq 11.7 \text{ M}_\odot$) the fraction is 54%. This difference may reflect the fact that it can be more difficult to recognize a type II AGN in a starburst due to the strong emission lines produced by star formation. The majority of UVLGs have the line ratios of normal star-forming galaxies. Note that type I AGN have been removed from the GR1/DR3 sample because the AGN would contribute significantly to the UV luminosity.

5. Discussion

5.1. Large and Compact UVLGs

The most luminous galaxies in the ultraviolet ($L_{1530} > 2 \times 10^{10} \text{ L}_\odot$) are a diverse population spanning a wide range of properties. Most of these properties are correlated at some level with the FUV surface brightness, which reflects the star formation rate per unit area. It is informative to use the surface brightness distribution to divide the UVLGs into two groups, “large” and “compact”.

The large UVLGs at the low surface brightness end are very massive spirals. They have stellar masses of $M_* > 10^{10.5} \text{ M}_\odot$, comparable to massive spirals in the local universe. They have half-light radii of 5 to 30 kpc. They are at the extreme end of the UV luminosity distribution, an indication that they have high global star formation rates. However, this high luminosity is a result of relatively modest star formation intensity spread out over a large area. They seem to share many of the characteristics of normal spirals but extend this population to high UV luminosity. By selecting the most luminous galaxies we have found the tail of the distribution of massive spirals.

The compact UVLGs at the high-surface brightness end are systems with intense star formation in a relatively compact region. They are lower mass systems ($M_* < 10^{10.5} \text{ M}_\odot$) with half-light radii of 1 to 5 kpc. They have high specific star formation rates, suggesting they may be experiencing their first major burst of star formation. They are generally metal-poor compared to the large UVLGs.

Figures 1 and 2 illustrate the basic differences between large and compact UVLGs. These figures show that the large UVLGs can be understood as the high-luminosity end of the distribution of normal galaxies. They are extremely luminous, but this is mostly a reflection of their large size. On the other hand, the compact UVLGs deviate from the trends established by the full sample, in that they are very luminous but not very large. Their high luminosity reflects an extremely high surface brightness in a relatively small region. This behavior sets them apart from the rest of the galaxies, and suggests that compact UVLGs are a distinct population of galaxies.

5.2. Local Analogs of Lyman Break Galaxies

One of the initial goals of this investigation was to find nearby galaxies with properties most similar to LBGs. To do this, we have defined a surface brightness cutoff at $I_{1530} > 10^9 L_{\odot} \text{ kpc}^{-2}$, which is the lower limit of UV surface brightness seen in typical LBGs (Giavalisco 2002). Table 2 shows that the galaxies in this sample (“supercompact UVLGs”) share all of the characteristics of LBGs that are considered in this paper, including UV luminosity, mass, star formation rate, specific star formation rate, UV attenuation, and metallicity. Like LBGs, they are compact systems undergoing intense star formation.

The question of whether this is the first major episode of star formation that these galaxies have undergone is crucial to determining how similar they are to LBGs. *Spitzer* observations of LBGs in the rest-frame near-IR have shown that they do not contain a previously hidden population of older, low-mass stars (Barmby et al. 2004). The UV-optical colors of many of the compact UVLGs suggest that this may be the first major episode of star formation these galaxies have experienced (see Figure 7). Near-infrared observations are necessary to fully trace the population of old stars. Such observations have been carried out with *Spitzer*, and will be reported in a forthcoming paper. The current UV-optical data, however, suggest that the compact UVLGs are indeed excellent local analogs to LBGs. Further study of these remarkable objects can provide crucial information about star formation in the early universe. Toward this end we are currently analyzing *Hubble Space Telescope* data (in addition to our *Spitzer* data) in order to study the morphologies, dust content, and stellar populations of compact UVLGs. The results from these studies will be presented in future papers.

Whether or not the highest surface brightness UVLGs are indeed analogs of LBGs, they are distinct from any previously studied population of galaxies in the local universe. They are much more luminous in the UV (and thus have much higher star formation rates) than blue compact dwarf galaxies (BCDGs), and have higher UV surface brightnesses (and thus star formation rates per unit area) than local starburst galaxies. For example, while I Zw 18, the prototypical BCDG, has an FUV surface brightness of $I_{1530} = 8.2 \times 10^7 L_{\odot} \text{ kpc}^{-2}$, which is close to the boundary for compact UVLGs, its FUV luminosity $L_{1530} = 1.7 \times 10^8 L_{\odot}$, more than 2 orders of magnitude below the lower limit for UVLGs (Gil de Paz et al. 2006).

Figure 12 compares the luminosity and surface brightness of galaxies in the *GALEX* Ultraviolet Atlas of Nearby Galaxies (Gil de Paz et al. 2006), including some nearby well-known starbursts and BCDGs, with the normalized distribution of the entire sample. The range in $\log L_{1530}$ for 14 starbursts from the atlas (not all shown in the figure) is from 8.2 to 10.5, and for 10 BCDGs in the atlas the range is 7.3 to 10.3. The boundary for UVLGs is $\log L_{1530} = 10.3$. In surface brightness the starbursts range from $\log I_{1530} = 6.2$ to 9.1, while the BCDGs range from 6.6 to 8.7. The Cartwheel galaxy, AM 0644-741, and UGC 06697 are three starburst galaxies that are also local examples of large UVLGs. Figure 12 shows that while some local galaxies have high FUV surface brightness, and others have high FUV luminosity, almost none have the combination of high luminosity and high surface brightness that would qualify as a compact UVLG. The exception is VV 114, which is the nearest known Lyman Break Galaxy analog (Grimes et al. 2006). Compact UVLGs, and especially supercompact UVLGs, clearly have extreme properties when compared to local galaxy populations.

6. Conclusions

We have used *GALEX* and the SDSS to identify and study the most UV luminous galaxies in the local universe. Our main results are as follows:

1. The most UV luminous galaxies in the local universe comprise a diverse group, with properties that are well correlated with UV surface brightness. Although there is not a sharp transition, we can use a surface brightness boundary of $I_{1530} < 10^8 L_{\odot} \text{ kpc}^{-2}$ to divide the UVLG sample into two groups: large and compact UVLGs.
2. The large UVLGs are massive, metal-rich disk galaxies with UV surface brightnesses only slightly larger than typical star forming galaxies. They are similar to normal galaxies in most respects, but are very luminous primarily because of their large size.
3. The compact UVLGs are low-mass, relatively metal-poor systems which often have a disturbed or interacting morphology. The high UV surface brightness and high specific star formation rate in these compact UVLGs indicates that intense star formation is ongoing.
4. It is possible to isolate a sample of local LBG-analogs with UV surface brightness criterion of $I_{1530} > 10^9 L_{\odot} \text{ kpc}^{-2}$. The galaxies in the resulting sample have many properties in common with LBGs, including luminosity, mass, star formation rate, specific star formation rate, extinction, and metallicity.
5. Compact UVLGs stand out from the trends established by the full DR3/GR1 sample in that they have much smaller sizes and higher surface brightness than would be predicted for galaxies of their mass or luminosity. They have metallicities that are generally lower by a factor of two to three compared to normal galaxies of the same mass. These properties suggest that they are a distinct population of objects, perhaps at a different phase of evolution than the bulk of the galaxies in the local universe.
6. The high UV luminosity and implied high star formation rate of compact UVLGs distinguishes them from any previously studied local galaxy population, including local UV-bright starbursts and blue compact dwarf galaxies.

We thank the referee, Michael Strauss, for providing very helpful comments that greatly improved the paper. *GALEX* is a NASA Small Explorer launched in April 2003. We gratefully acknowledge NASA's support for construction, operation, and scientific analysis for the *GALEX* mission. Funding for the creation and distribution of the SDSS Archive has been provided by the Alfred P. Sloan Foundation, the Participating Institutions, the National Aeronautics and Space Administration, the National Science Foundation, the U.S. Department of Energy, the Japanese Monbukagakusho, and the Max Planck Society.

REFERENCES

- Abazajian, K., et al. 2003, *AJ*, 126, 2081
- Abazajian, K., et al. 2005, *AJ*, 129, 1755
- Arnouts, S., et al. 2005, *ApJ*, 619, L43
- Baldwin, J. A., Phillips, M. M., & Terlevich, R. 1981, *PASP*, 93, 5
- Barmby, P., et al. 2004, *ApJS*, 154, 97
- Bianchi, L., et al. 2006, *ApJS*, this volume

- Brinchmann, J., Charlot, S., White, S. D. M., Tremonti, C., Kauffmann, G., Heckman, T., & Brinkmann, J. 2004, MNRAS, 351, 1151
- Bruzual, G., & Charlot, S. 2003, MNRAS, 344, 1000
- Calzetti, D. 2001, PASP, 113, 1449
- Charlot, S., & Fall, S. M. 2000, ApJ, 539, 718
- Charlot, S., & Longhetti, M. 2001, MNRAS, 323, 887
- Dickinson, M., et al. 2004, ApJ, 600, L99
- Erb, D. K., Steidel, C. C., Shapley, A. E., Pettini, M., Reddy, N. A., & Adelberger, K. L. 2006, ApJ, 646, 107
- Erb, D. K., Shapley, A. E., Pettini, M., Steidel, C. C., Reddy, N. A., & Adelberger, K. L. 2006, ApJ, 644, 813
- Ferguson, H., et al. 2004, ApJ, 600, L107
- Giavalisco, M. 2002, ARA&A, 40, 579
- Giavalisco, M., et al. 2004, ApJ, 600, L103
- Gil de Paz, A., et al. 2006, ApJS, this volume
- Grimes, J. P., Heckman, T. M., Hoopes, C. G., Strickland, D. K., Aloisi, A., Meurer, G., Ptak, A. 2006, ApJ, 648, 310
- Heckman, T. M., Robert, C., Leitherer, C., Garnett, D. R., & van der Rydt, F. 1998, ApJ, 503, 646
- Heckman, T.M., et al. 2005, ApJ, 619, L35; Paper I
- Kauffmann, G., et al. 2003a, MNRAS, 341, 33
- Kauffmann, G., et al. 2003b, MNRAS, 341, 54
- Kauffmann, G., et al. 2003c, MNRAS, 346, 1055
- Kennicutt, R. C., Jr. 1998, ARA&A, 36, 189
- Madau, P., Ferguson, H. C., Dickinson, M. E., Giavalisco, M., Steidel, C. C., & Fruchter, A. 1996, MNRAS, 283, 1388
- Martin, D. C., et al. 2005, ApJ, 619, L1
- Morrisey, P. F., et al. 2004, ApJ, 619 L7
- Meurer, G. R., Heckman, T. M., & Calzetti, D. 1999, ApJ, 521, 64
- Papovich, C., Dickinson, M., & Ferguson, H. 2001, ApJ, 559, 620
- Pettini, M. & Pagel, B. E. 2004, MNRAS, 348, L59
- Reddy, N. A., et al. 2006, ApJ, in press [astro-ph/0602596]

- Salim, S., et al. 2005, *ApJ*, 619, L39
- Savaglio, S., et al. 2005, *ApJ*, 635, 260
- Schiminovich, D., et al. 2005, *ApJ*, 619, L47
- Shapley, A. E., Coil, A. L., Ma, C.-P., & Bundy, K. 2005, *ApJ*, 635, 1006
- Shapley, A. E., Erb, D. K., Pettini, M., Steidel, C. C., & Adelberger, K. L. 2004, *ApJ*, 612, 108
- Shapley, A., Steidel, C., Adelberger, K., Dickinson, M., Giavalisco, M., & Pettini, M. 2001, *ApJ*, 562, 95
- Steidel, C. C., Adelberger, K. L., Giavalisco, M., Dickinson, M., & Pettini, M. 1999, *ApJ*, 519, 1
- Steidel, C. C., Adelberger, K. L., Shapley, A. E., Pettini, M., Dickinson, M., & Giavalisco, M. 2003, *ApJ*, 592, 728
- Steidel, C. C., Giavalisco, M., Pettini, M., Dickinson, M., & Adelberger, K. L. 1996, *ApJ*, 462, L17
- Steidel, C. C., & Hamilton, D. 1993, *AJ*, 105, 2017
- Tremonti, C. A., et al. 2004, *ApJ*, 613, 898
- Wyder, T. K., et al. 2005, *ApJ*, 619, L15

Table 1. UVLG Sample

SDSS ObjID	RA (deg)	Dec (deg)	Redshift	$\log L_{1530}$ (L_{\odot})	$r_{50,u}$ (kpc)	$\log I_{1530}$ ($L_{\odot} \text{ kpc}^{-2}$)	FUV (mag)	NUV (mag)	A_{1530} (mag)	$\log M_{*}$ (M_{\odot})	$\log \text{SFR}$ ($M_{\odot} \text{ yr}^{-1}$)	$12+\log(\text{O}/\text{H})$
(1)	(2)	(3)	(4)	(5)	(6)	(7)	(8)	(9)	(10)	(11)	(12)	(13)
587731187814629504	0.20128	1.15675	0.250	10.34	3.13	8.55	20.51±0.25	20.16±0.15	0.80	10.08	1.03	8.89
588015508196294786	1.46632	-0.73521	0.134	10.34	9.62	7.58	19.02±0.28	20.09±0.26	3.25	10.76	0.76	...
58801550765954916	1.77391	-1.07124	0.288	10.51	5.14	8.29	20.44±0.25	20.34±0.17	1.51	10.67	1.44	8.89
587731185131192547	2.40203	-0.84206	0.161	10.42	7.69	7.85	19.26±0.15	18.87±0.08	2.26	10.56	0.60	9.02
587727225154306171	2.45330	-11.03518	0.211	10.35	4.13	8.32	20.08±0.22	19.55±0.10	1.42	9.98	1.07	8.67
588015508196753479	2.54157	-0.76765	0.243	10.45	1.38	9.37	20.19±0.23	19.86±0.15	1.00	10.43	1.18	8.74
588015510344302646	2.78681	0.84544	0.108	10.54	3.24	8.72	18.02±0.08	17.87±0.04	0.37	9.76	1.71	8.71
588015509270626537	2.86065	0.06754	0.211	10.36	6.55	7.93	20.07±0.22	19.86±0.11	2.96	10.62	1.15	9.02
587727225154764940	3.43824	-10.93658	0.246	10.57	12.52	7.58	19.90±0.08	19.27±0.03	2.35	10.99	1.20	9.06
587727225154961583	3.99757	-11.02590	0.267	10.40	23.68	6.85	20.53±0.07	19.99±0.03	2.21	11.62	0.95	...
587731185132109826	4.36789	-0.94027	0.094	10.32	2.70	8.66	18.25±0.09	17.92±0.05	1.73	10.74	1.25	8.96
587731185132241048	4.78147	-0.87711	0.187	10.42	4.13	8.39	19.63±0.17	19.35±0.10	1.37	10.28	1.35	8.89
587727227304476771	8.60397	-9.19877	0.164	10.47	8.98	7.77	19.17±0.04	19.57±0.04	1.70	10.76	0.45	...
587727180600705169	8.71946	-9.02820	0.144	10.38	10.40	7.55	19.09±0.14	18.83±0.07	2.27	10.27	0.66	8.96
587727177916416108	8.84842	-11.12945	0.123	10.33	9.98	7.53	18.83±0.03	20.19±0.03	2.85	10.44	-0.13	...
587724198812057678	9.06934	15.04284	0.119	10.63	3.99	8.63	18.02±0.03	...	1.91	10.61	0.21	9.11
587727225157386334	9.58818	-10.88660	0.184	10.52	9.26	7.79	19.34±0.15	19.13±0.08	2.18	10.77	1.06	8.94
587724199349387411	10.22635	15.56938	0.283	10.43	1.72	9.16	20.62±0.08	21.03±0.05	0.13	9.18	0.41	8.23
587724199349518558	10.52352	15.36599	0.259	10.32	13.81	7.24	20.66±0.10	20.28±0.04	9.20	11.27	0.91	...
588015509274165442	10.94763	0.05960	0.213	10.83	13.08	7.80	18.92±0.11	18.94±0.08	0.63	11.24	0.84	...
587724199349780648	11.19722	15.48662	0.227	10.56	2.30	9.04	19.75±0.05	19.52±0.03	...	10.71	1.39	...
588015510348169371	11.61157	0.86546	0.166	10.42	2.86	8.71	19.34±0.14	18.74±0.06	1.31	10.41	1.13	8.60
587724233712140399	11.69467	15.72774	0.181	10.43	9.28	7.70	19.52±0.05	19.16±0.02	3.41	11.10	1.06	9.27
587724232101724283	12.19103	14.44148	0.278	10.40	4.04	8.39	20.64±0.31	20.46±0.21	1.97	11.00	1.92	...
588015508738539596	13.86443	-0.36355	0.167	10.49	0.80	9.89	19.19±0.14	18.72±0.07	...	10.07	1.18	...
587727179529322564	14.14723	-9.82308	0.189	10.58	4.74	8.43	19.23±0.04	...	0.00	11.08	0.57	9.01
587731187283853386	14.19609	0.64680	0.218	10.43	2.38	8.88	19.96±0.20	19.30±0.12	1.38	10.02	0.92	8.65
587724234250256545	14.69203	16.03578	0.243	10.36	4.18	8.32	20.41±0.28	19.76±0.16	1.47	10.17	0.78	8.72
587724199888289961	14.98405	15.64598	0.144	11.16	11.24	8.26	17.14±0.02	19.11±0.02	1.99	10.94	0.53	...
587724197204132105	15.36074	13.54601	0.223	10.51	11.28	7.61	19.82±0.20	19.72±0.15	10.44	11.10	0.69	...
587724198814810262	15.61241	14.91062	0.086	10.33	1.68	9.08	18.00±0.03	...	0.66	9.93	-0.29	8.89
587731511530815637	16.03357	-0.84219	0.207	10.38	4.08	8.36	19.96±0.23	19.29±0.09	0.80	10.09	1.44	8.78
588015509276590315	16.56369	0.12798	0.220	10.41	8.69	7.73	20.04±0.22	19.94±0.12	1.83	10.86	0.78	9.11
587731514215497820	16.70578	1.05622	0.253	10.95	5.02	8.75	19.04±0.14	19.69±0.11	1.43	11.70	2.41	...
587731514215497878	16.80949	1.15869	0.159	10.34	6.82	7.87	19.43±0.17	19.55±0.10	2.01	10.78	0.91	9.14
587724197204983886	17.31450	13.43438	0.184	10.55	12.58	7.55	19.25±0.16	19.02±0.09	...	11.48	1.63	...
587724233178808483	20.14169	14.77605	0.130	10.48	11.91	7.53	18.61±0.03	...	3.26	11.07	0.53	...
587724233179332766	21.25810	14.63618	0.153	10.37	8.52	7.71	19.26±0.04	18.81±0.02	2.63	11.12	1.23	...
587727180069404773	21.54104	-9.12973	0.263	10.38	30.63	6.61	20.55±0.07	20.08±0.05	2.23	11.70	0.99	...
587727178460496000	25.59877	-10.18952	0.128	10.41	3.47	8.53	18.72±0.03	18.41±0.01	0.56	9.56	0.55	8.67

Table 1—Continued

SDSS ObjID	RA (deg)	Dec (deg)	Redshift	$\log L_{1530}$ (L_{\odot})	$r_{50,u}$ (kpc)	$\log I_{1530}$ ($L_{\odot} \text{ kpc}^{-2}$)	FUV (mag)	NUV (mag)	A_{1530} (mag)	$\log M_{*}$ (M_{\odot})	$\log \text{SFR}$ ($M_{\odot} \text{ yr}^{-1}$)	$12+\log(\text{O}/\text{H})$
(1)	(2)	(3)	(4)	(5)	(6)	(7)	(8)	(9)	(10)	(11)	(12)	(13)
587724233181429914	26.26956	14.25279	0.172	10.36	9.84	7.58	19.57±0.05	19.36±0.02	0.00	11.14	-0.20	...
587727229449338983	26.80144	-10.21155	0.198	10.35	14.62	7.22	19.92±0.05	19.31±0.02	0.00	11.06	0.86	...
587724232644821098	26.81554	13.91049	0.193	10.47	3.21	8.66	19.58±0.05	19.03±0.02	0.48	10.08	1.44	8.70
587724197746180186	27.61831	13.14958	0.147	10.62	1.66	9.38	18.55±0.03	18.26±0.02	1.26	10.42	0.91	8.87
587724232108409001	27.85828	13.41965	0.243	10.52	1.53	9.35	20.00±0.06	19.53±0.03	1.19	10.52	1.29	8.98
587724197746376839	27.95274	13.19747	0.191	10.60	7.58	8.04	19.21±0.05	...	2.21	11.32	-0.01	...
587724233720004940	30.32127	14.33144	0.285	10.34	54.49	6.07	20.86±0.09	19.91±0.03	3.55	11.10	-0.07	9.10
587724198822215805	32.98133	13.47305	0.149	10.33	14.74	7.20	19.30±0.05	18.83±0.02	1.79	11.23	0.90	...
587724232647508116	33.09660	13.20805	0.134	10.34	13.95	7.25	19.02±0.04	18.59±0.02	3.75	11.21	0.99	...
587724198285541435	33.45223	12.99766	0.219	10.58	0.85	9.92	19.59±0.06	18.72±0.02	2.48	10.68	1.35	...
587731511538745437	34.13192	-1.02454	0.167	10.39	3.43	8.52	19.41±0.16	18.88±0.07	1.44	10.34	1.51	8.85
587727179540463751	39.85733	-8.14107	0.184	10.99	13.21	7.95	18.16±0.03	18.71±0.01	6.02	11.40	0.06	...
587727179540594732	40.14347	-8.15686	0.177	10.31	5.77	7.99	19.74±0.05	19.27±0.02	1.36	10.51	0.76	9.00
587724241226498139	41.37314	-8.27718	0.195	10.41	1.66	9.17	19.74±0.05	19.08±0.03	1.39	10.36	1.36	8.83
587724240153018558	42.18780	-8.96868	0.238	10.73	20.17	7.32	19.42±0.04	19.28±0.03	2.33	10.99	0.98	9.00
587724241226891413	42.38908	-8.09707	0.270	11.11	24.91	7.52	18.77±0.03	18.63±0.02	2.03	10.73	1.78	8.61
587731511543464076	44.95400	-0.96678	0.293	10.59	5.14	8.37	20.30±0.23	19.47±0.11	1.95	10.96	1.93	8.87
588015509825978540	45.13415	0.51732	0.170	10.38	3.36	8.53	19.48±0.14	19.76±0.11	2.61	10.84	1.00	...
587727180616695902	45.53338	-6.63504	0.180	10.42	12.46	7.43	19.52±0.20	19.18±0.10	1.62	10.94	0.85	8.87
587727179543740592	47.44834	-7.33566	0.196	10.43	4.96	8.24	19.71±0.06	19.58±0.03	2.26	10.58	0.95	9.06
587724241766187109	47.84834	-7.00088	0.226	10.44	11.45	7.52	20.02±0.06	19.76±0.03	2.14	11.33	0.83	8.98
587724241229643897	48.61778	-7.42162	0.208	10.32	2.02	8.91	20.12±0.08	20.09±0.04	0.78	10.46	0.29	...
587724240156360834	49.81060	-8.06979	0.125	10.50	3.21	8.69	18.45±0.12	18.25±0.07	1.79	10.29	1.00	8.88
587731511545954498	50.61609	-1.03658	0.194	10.31	14.16	7.21	19.98±0.28	20.19±0.30	2.94	10.94	0.51	...
587731514230571148	51.21346	1.11823	0.150	10.31	12.84	7.29	19.35±0.20	19.24±0.20	1.10	11.03	0.31	...
588015510365602004	51.34779	0.96633	0.212	10.33	12.41	7.34	20.15±0.29	20.30±0.26	0.53	11.21	0.80	9.31
587731512083415213	51.98476	-0.47176	0.162	10.54	4.53	8.43	18.97±0.16	18.62±0.09	0.90	10.29	1.64	8.83
587731512620351653	52.09571	-0.13294	0.205	10.31	3.32	8.47	20.12±0.30	19.70±0.18	0.81	9.95	1.28	8.85
587731514231029883	52.19166	1.19744	0.142	10.39	1.74	9.11	19.04±0.17	19.05±0.12	0.48	9.74	1.19	8.78
587724242305286402	52.93439	-5.93593	0.247	10.52	2.76	8.84	20.03±0.06	19.60±0.04	0.33	9.79	1.31	8.61
587731513694617768	53.22892	0.64229	0.227	10.54	12.33	7.56	19.78±0.24	19.42±0.17	1.51	11.14	0.89	9.02
588015509292712195	53.34551	0.09876	0.178	10.49	8.30	7.85	19.32±0.17	...	4.56	11.03	0.57	...
587731514231750803	53.87266	1.24974	0.171	10.48	6.96	8.00	19.25±0.21	19.93±0.24	1.49	10.63	0.68	9.14
587731514232144016	54.77985	1.16598	0.182	10.36	6.40	7.95	19.71±0.25	20.03±0.31	2.33	10.89	0.68	9.03
587731514232144028	54.80193	1.13992	0.261	10.62	3.60	8.71	19.94±0.27	19.64±0.18	2.05	10.90	1.15	9.07
588015510367240313	55.09066	0.92732	0.253	10.36	5.70	8.05	20.52±0.30	19.75±0.20	1.43	10.59	1.07	9.03
587731513158991989	56.09607	0.39638	0.219	10.32	4.04	8.31	20.25±0.30	19.78±0.14	1.53	10.33	1.60	8.82
587724242307121309	57.03210	-5.42077	0.164	10.38	4.91	8.20	19.38±0.19	19.19±0.12	0.62	10.04	1.17	8.58
587724240697622665	59.81242	-6.30119	0.181	10.51	8.05	7.90	19.30±0.19	19.21±0.15	3.03	11.07	1.41	8.98
587727180086378659	60.53695	-5.11169	0.139	10.45	1.20	9.49	18.85±0.15	18.88±0.09	0.23	9.39	1.22	8.53

Table 1—Continued

SDSS ObjID	RA (deg)	Dec (deg)	Redshift	$\log L_{1530}$ (L_{\odot})	$r_{50,u}$ (kpc)	$\log I_{1530}$ ($L_{\odot} \text{ kpc}^{-2}$)	FUV (mag)	NUV (mag)	A_{1530} (mag)	$\log M_{*}$ (M_{\odot})	$\log \text{SFR}$ ($M_{\odot} \text{ yr}^{-1}$)	$12+\log(\text{O}/\text{H})$
(1)	(2)	(3)	(4)	(5)	(6)	(7)	(8)	(9)	(10)	(11)	(12)	(13)
588007005229875657	115.76499	37.73554	0.202	10.44	5.97	8.09	19.74±0.05	19.31±0.02	2.13	11.44	1.05	9.11
587735236344414396	120.41840	23.20090	0.272	10.33	3.85	8.36	20.76±0.30	19.65±0.10	2.69	10.78	1.31	9.06
587728668268167253	122.18443	39.81455	0.091	10.45	0.50	10.25	17.85±0.08	17.54±0.04	1.04	10.33	1.02	...
587725981224599567	123.84753	50.07076	0.164	10.50	1.87	9.16	19.11±0.15	18.61±0.07	1.51	10.30	2.10	8.99
587725774535000285	124.04864	49.38725	0.179	10.47	12.72	7.46	19.37±0.17	19.17±0.09	3.12	11.30	1.23	...
587725470130110508	124.34376	46.74989	0.280	10.83	3.24	9.01	19.57±0.05	19.13±0.02	0.48	9.98	1.53	8.68
588007004697854025	124.67503	46.58495	0.218	10.43	2.24	8.93	19.97±0.05	19.31±0.02	3.02	11.21	2.21	9.06
587728668806611190	124.74548	42.90008	0.154	10.43	13.09	7.40	19.13±0.15	18.87±0.08	1.73	11.25	0.77	...
587728931875651786	124.86896	41.29362	0.179	10.41	6.86	7.94	19.55±0.18	19.88±0.12	1.96	10.82	1.42	9.11
587728664505483532	124.88740	42.60294	0.232	10.53	2.86	8.82	19.86±0.21	20.28±0.15	1.20	10.98	0.50	...
588007004160983209	125.22800	46.21449	0.229	10.41	2.96	8.67	20.13±0.06	19.63±0.03	1.16	9.79	1.13	8.66
587731872314884117	125.40520	37.17965	0.284	10.80	1.84	9.47	19.70±0.12	19.27±0.07	0.58	9.99	1.54	8.89
587728664506073210	126.05471	43.62250	0.118	10.61	2.64	8.97	18.05±0.09	17.90±0.05	...	10.36	1.40	...
587728931876176092	126.06725	42.16934	0.223	10.34	10.02	7.54	20.24±0.24	...	2.11	11.13	-2.05	...
587731885736788122	126.13889	38.00366	0.103	10.33	4.37	8.25	18.43±0.07	17.84±0.03	1.22	10.93	1.71	9.15
587728664506400946	126.71116	44.14319	0.132	10.35	11.51	7.43	18.97±0.13	18.31±0.07	1.53	11.05	0.82	...
587731886275166445	128.88380	40.71084	0.084	10.31	4.06	8.30	18.01±0.08	17.94±0.05	0.44	9.67	0.52	8.61
588010136800395436	129.38982	47.96454	0.215	10.56	2.96	8.82	19.59±0.15	18.93±0.06	0.30	9.91	1.41	8.31
588010135726456918	129.61571	47.17575	0.097	10.38	2.07	8.95	18.17±0.01	17.73±0.01	1.35	10.72	0.80	8.88
588009365859074276	130.71088	46.97751	0.229	10.33	11.08	7.44	20.33±0.04	19.66±0.02	2.79	11.15	1.09	...
587728931341336751	130.91106	45.25332	0.193	10.42	4.74	8.27	19.68±0.16	19.46±0.08	2.39	10.65	1.43	9.10
587725470670192770	131.50928	52.53307	0.053	10.31	3.95	8.32	16.95±0.01	16.50±0.00	2.24	11.15	1.06	9.20
587728930804859108	132.25192	45.56725	0.220	10.58	10.79	7.72	19.61±0.16	19.34±0.08	2.85	11.03	0.88	9.08
587725552275226831	133.40443	57.07639	0.299	11.33	32.03	7.52	18.48±0.03	11.53	-0.17	...
587732049480056879	136.07295	45.62538	0.195	10.47	9.68	7.70	19.58±0.20	19.34±0.10	2.70	10.85	0.99	9.11
587725469598023726	136.63254	54.47703	0.205	10.41	2.58	8.79	19.86±0.17	19.23±0.08	1.00	10.15	1.61	8.85
587732702855627062	136.67363	5.37485	0.226	10.33	9.72	7.56	20.30±0.26	20.07±0.17	2.80	11.29	0.99	...
587732701782016286	137.08205	4.58679	0.124	10.35	9.05	7.64	18.82±0.14	18.24±0.06	2.43	10.74	0.90	9.06
588007004703096884	137.59975	55.39899	0.171	10.33	2.24	8.83	19.62±0.04	19.04±0.02	2.21	11.00	1.37	...
587727942954844494	137.80559	1.23246	0.252	10.32	32.82	6.49	20.60±0.07	20.29±0.03	4.55	11.31	0.53	...
587732054319890553	139.35410	42.75827	0.237	10.31	7.26	7.79	20.45±0.22	19.81±0.11	2.50	11.09	1.27	...
587725817477988424	139.44617	59.29116	0.173	10.38	2.43	8.81	19.54±0.17	18.66±0.07	1.78	10.56	1.27	8.91
587731913110257902	139.95036	48.64304	0.237	10.32	14.44	7.20	20.43±0.25	19.88±0.11	1.76	11.01	0.91	9.04
587725551740321978	140.07605	59.86119	0.195	10.39	10.64	7.54	19.78±0.19	19.71±0.13	2.34	10.90	0.77	9.05
587731521208582257	140.49748	45.15344	0.235	10.82	1.53	9.65	19.17±0.13	18.80±0.06	2.22	10.54	1.99	...
587725551203451103	140.60236	59.61079	0.277	10.40	16.56	7.16	20.63±0.27	20.18±0.17	2.30	11.47	0.57	...
588007004167012515	140.65002	56.27194	0.191	10.32	6.25	7.93	19.91±0.19	19.23±0.08	3.15	11.10	1.28	9.11
587731913110520003	140.65392	48.95396	0.185	10.42	16.01	7.21	19.60±0.16	19.10±0.07	0.84	11.09	0.58	...
588010136804786207	140.90192	54.81091	0.222	10.56	1.14	9.65	19.68±0.17	19.45±0.10	1.36	9.97	0.85	8.86
587725470673535009	141.13921	57.73800	0.227	10.69	9.29	7.96	19.42±0.16	...	2.28	11.18	0.75	8.98

Table 1—Continued

SDSS ObjID	RA	Dec	Redshift	$\log L_{1530}$	$r_{50,u}$	$\log I_{1530}$	FUV	NUV	A_{1530}	$\log M_*$	$\log \text{SFR}$	$12+\log(\text{O}/\text{H})$
(1)	(deg)	(deg)	(4)	(L_\odot)	(kpc)	($L_\odot \text{ kpc}^{-2}$)	(mag)	(mag)	(mag)	(M_\odot)	($M_\odot \text{ yr}^{-1}$)	(13)
588013384341913605	141.50169	44.46005	0.181	10.73	1.03	9.91	18.76±0.10	18.84±0.06	0.46	9.20	0.72	8.46
587731521746043150	141.68233	46.17589	0.154	10.31	12.61	7.31	19.41±0.15	19.19±0.08	1.45	10.55	0.64	...
588007006315544766	142.18282	59.00600	0.226	10.62	27.68	6.94	19.57±0.04	19.34±0.02	0.34	10.54	2.46	8.77
587729385531310202	142.37518	50.58275	0.223	10.46	11.44	7.54	19.94±0.22	19.62±0.10	2.87	10.98	0.89	9.10
587731680122110146	142.46309	46.42466	0.188	10.33	8.15	7.71	19.85±0.18	...	0.90	10.26	0.98	8.86
587725816405098641	143.44133	59.84856	0.231	10.37	1.98	8.98	20.25±0.23	19.86±0.11	0.41	9.70	1.00	8.70
587732484347723780	143.78641	42.78500	0.234	10.59	2.76	8.91	19.74±0.17	19.36±0.09	1.62	10.21	1.36	8.81
587728932420255860	143.99200	53.45718	0.199	10.38	8.38	7.74	19.86±0.17	19.45±0.08	1.55	10.86	1.05	9.11
588009365863989360	143.99982	54.36830	0.262	10.69	5.77	8.37	19.76±0.17	19.17±0.07	1.71	10.88	1.64	...
588009367475847371	147.05156	56.99398	0.214	10.31	14.44	7.19	20.20±0.21	20.26±0.12	2.64	11.00	1.03	...
587725816943083550	147.10237	61.66580	0.173	10.43	1.04	9.60	19.39±0.04	19.28±0.02	...	9.88	0.92	...
587725816406081719	147.16391	61.22299	0.185	10.91	8.46	8.26	18.36±0.03	...	1.95	10.82	0.24	...
587731868014084272	147.40846	47.39235	0.249	10.36	6.32	7.96	20.47±0.23	20.51±0.17	2.20	10.61	1.10	9.06
587731869088219192	147.90614	48.66147	0.135	10.39	1.89	9.04	18.91±0.11	18.99±0.07	0.56	9.46	0.49	8.25
588010135732814044	147.92696	56.43008	0.283	10.38	6.04	8.02	20.72±0.27	20.31±0.12	1.48	10.68	1.07	9.11
588009367476174965	148.14238	57.40535	0.257	10.49	3.90	8.51	20.22±0.21	19.71±0.09	1.74	10.78	2.35	9.00
587732049484513320	148.64407	51.58557	0.130	10.78	1.55	9.60	17.84±0.07	...	0.89	9.56	1.35	8.63
587735241719021680	148.73982	39.74292	0.198	10.46	9.21	7.73	19.64±0.15	19.27±0.08	2.61	11.08	1.26	...
588009367476306065	148.80473	57.53416	0.141	10.40	2.46	8.82	18.99±0.12	19.22±0.08	0.19	9.62	0.82	8.60
588016526633861363	149.22546	38.67062	0.205	10.40	8.84	7.71	19.90±0.18	19.85±0.10	1.58	10.85	0.55	...
588009367476568126	149.58009	57.82781	0.201	10.42	12.82	7.41	19.78±0.17	19.52±0.10	2.84	11.20	0.86	...
587735239571603546	149.87546	38.15611	0.211	10.31	9.22	7.58	20.17±0.20	19.72±0.09	3.47	10.87	1.04	9.13
588009365865758909	150.09341	56.59479	0.228	10.31	10.50	7.47	20.37±0.22	20.08±0.13	2.20	11.03	1.08	...
587735239571669282	150.10429	38.41888	0.252	10.41	12.81	7.40	20.36±0.22	20.37±0.13	3.54	11.13	1.33	9.08
587729387144806501	150.50368	55.12448	0.247	10.45	5.26	8.21	20.21±0.20	19.58±0.09	2.42	11.09	1.70	...
588297864722382971	152.10156	42.73342	0.181	10.33	4.58	8.21	19.76±0.18	19.72±0.10	2.55	10.78	0.73	9.06
587732482202861656	152.16473	44.11267	0.151	10.56	11.73	7.62	18.76±0.10	18.55±0.05	0.59	11.05	0.64	...
587732135914045580	152.51022	48.11020	0.255	10.44	15.28	7.27	20.33±0.22	20.13±0.16	2.05	11.40	0.65	...
587732135377109127	152.62944	47.70260	0.190	10.46	7.01	7.97	19.56±0.15	19.40±0.08	2.44	10.78	1.22	9.07
587732136451047490	152.72443	48.49102	0.158	10.34	3.32	8.50	19.42±0.14	19.74±0.10	2.18	10.78	0.31	...
587725816944459876	153.04662	63.41769	0.246	10.33	1.23	9.35	20.50±0.23	20.08±0.11	0.59	9.84	1.02	8.76
587732483814129906	153.54796	45.79028	0.161	10.38	11.82	7.44	19.37±0.14	18.97±0.06	1.80	11.02	0.81	...
587729388219662459	153.73042	57.11367	0.255	10.35	10.92	7.48	20.53±0.24	19.93±0.10	4.46	11.21	0.93	9.15
587732152571986075	153.91460	45.34412	0.211	10.34	12.79	7.33	20.10±0.19	19.70±0.09	8.48	11.48	0.66	...
588009368551817353	154.89285	60.22631	0.156	10.31	14.23	7.21	19.44±0.14	19.53±0.10	1.42	11.23	0.43	...
587731500796739661	155.78958	54.49640	0.214	10.37	9.54	7.61	20.07±0.20	19.74±0.09	0.00	11.22	0.55	...
587731869090709644	155.85841	51.10234	0.138	10.40	5.64	8.10	18.95±0.12	18.66±0.06	1.00	10.08	0.85	8.82
587732048949739624	156.04276	53.32828	0.185	10.40	10.56	7.55	19.65±0.16	19.28±0.08	0.69	11.03	0.82	9.05
587732048412868688	156.30435	52.87869	0.177	10.31	12.45	7.32	19.76±0.17	19.53±0.10	1.76	10.96	1.09	...
587732582053117989	156.54250	56.66665	0.197	10.32	7.57	7.76	20.00±0.18	...	4.31	11.24	0.62	...

Table 1—Continued

SDSS ObjID	RA (deg)	Dec (deg)	Redshift	$\log L_{1530}$ (L_{\odot})	$r_{50,u}$ (kpc)	$\log I_{1530}$ ($L_{\odot} \text{ kpc}^{-2}$)	FUV (mag)	NUV (mag)	A_{1530} (mag)	$\log M_{*}$ (M_{\odot})	$\log \text{SFR}$ ($M_{\odot} \text{ yr}^{-1}$)	$12+\log(\text{O}/\text{H})$
(1)	(2)	(3)	(4)	(5)	(6)	(7)	(8)	(9)	(10)	(11)	(12)	(13)
587732135378354188	156.55821	48.74970	0.160	10.47	2.17	9.00	19.13±0.12	18.91±0.06	0.25	9.91	1.10	8.33
588013383810220184	157.34006	49.69535	0.194	10.35	11.42	7.44	19.88±0.17	19.95±0.10	2.49	10.81	0.60	...
587731870701977714	157.43727	52.86215	0.227	10.36	6.85	7.89	20.24±0.21	20.06±0.13	3.37	11.05	1.94	9.06
588009370685276243	157.76656	58.93386	0.173	10.44	2.46	8.86	19.37±0.17	18.72±0.07	...	10.13	1.42	8.70
588007005245472903	157.82327	62.65335	0.198	10.39	4.69	8.25	19.83±0.17	20.10±0.13	1.40	10.90	0.70	...
588007005782540350	158.33391	63.18797	0.145	10.62	5.32	8.37	18.50±0.09	18.18±0.05	2.25	10.99	2.10	9.06
587725551744909441	159.76553	65.55137	0.117	10.43	7.33	7.90	18.47±0.09	18.17±0.05	2.70	10.82	1.07	9.12
587732049487790084	159.83974	54.78919	0.186	10.57	2.92	8.84	19.21±0.13	18.62±0.05	0.09	9.54	1.13	8.62
587729386073489559	160.15704	56.81467	0.148	10.32	3.03	8.56	19.29±0.16	19.22±0.09	0.15	10.64	1.67	8.85
587725817483034723	160.69228	65.39616	0.189	10.34	9.44	7.59	19.84±0.05	19.18±0.02	1.59	11.04	1.45	9.13
587725551745564802	162.93958	66.10591	0.170	10.31	0.86	9.64	19.65±0.04	19.30±0.02	1.08	9.57	1.15	8.83
587725819094696047	165.08723	67.48546	0.191	10.33	5.02	8.13	19.90±0.23	19.42±0.10	1.50	11.19	1.37	9.14
587729386075455636	168.17336	58.13764	0.154	10.36	11.11	7.47	19.29±0.13	18.80±0.06	1.82	11.11	1.03	...
587729153595539594	169.57059	63.26297	0.238	10.38	2.24	8.88	20.30±0.22	20.42±0.13	1.27	10.23	1.34	8.91
588011099410071613	169.80771	62.91817	0.286	10.32	4.04	8.31	20.90±0.28	20.27±0.12	0.75	10.95	0.67	...
587729155743875234	173.26578	65.22815	0.241	10.72	0.38	10.77	19.48±0.04	19.62±0.02	0.01	8.94	0.51	8.19
588009372836757702	174.94957	63.15313	0.245	10.41	1.98	9.02	20.29±0.23	20.47±0.14	1.59	10.40	1.11	...
587725816412766387	180.20340	66.43546	0.120	10.35	8.36	7.71	18.73±0.10	18.61±0.06	1.86	11.05	0.71	9.10
587728677395234987	189.59756	64.20047	0.212	10.38	10.17	7.57	20.00±0.21	19.87±0.11	0.25	11.12	0.97	...
587728677932105821	189.88033	64.68499	0.133	10.50	1.48	9.36	18.60±0.11	...	0.52	9.83	0.94	8.62
587725552827105291	208.48289	66.80015	0.198	10.66	1.89	9.31	19.16±0.13	18.48±0.05	0.84	9.99	1.71	8.72
588848899930194109	219.96780	-0.07335	0.203	10.34	10.99	7.46	20.01±0.08	19.77±0.04	2.37	10.91	0.69	...
587725575888634103	260.11795	59.22827	0.221	10.46	12.54	7.47	19.92±0.06	...	2.39	11.40	0.17	...
587725575888634081	260.18839	59.27158	0.154	10.31	7.50	7.76	19.42±0.04	19.00±0.02	2.34	10.66	0.82	9.02
587725576425505123	261.11240	59.28925	0.255	10.50	9.42	7.75	20.17±0.06	19.83±0.04	0.84	11.31	0.96	...
587730847960924833	312.50006	0.52355	0.164	10.37	0.60	10.01	19.42±0.23	19.67±0.18	1.47	10.65	0.93	...
587730846887707478	313.79340	-0.31749	0.198	10.41	2.52	8.81	19.78±0.24	18.74±0.09	1.09	10.25	1.00	8.74
587730847962104313	315.19748	0.55589	0.254	10.59	6.32	8.19	19.93±0.24	19.85±0.14	1.26	11.25	1.33	...
587730848499237044	315.84958	0.99881	0.177	10.32	7.51	7.77	19.72±0.31	19.53±0.17	4.22	11.15	1.51	...
587727212271567298	317.70895	-8.01180	0.211	10.39	21.74	6.92	19.98±0.08	19.76±0.04	6.37	11.15	0.63	...
587730847428510324	322.76953	0.09779	0.178	10.33	7.76	7.75	19.72±0.18	19.65±0.12	2.25	10.56	0.93	9.06
587730846891704703	322.89319	-0.30288	0.213	10.66	10.84	7.79	19.33±0.14	19.84±0.16	2.37	11.44	0.63	...
587727212273992007	323.27859	-8.59399	0.217	10.51	9.72	7.74	19.76±0.19	20.17±0.13	3.08	11.16	0.70	...
587731186725814690	325.83533	0.25139	0.169	10.37	13.48	7.31	19.50±0.19	19.16±0.13	0.00	11.37	0.60	...
587731187799687683	326.06918	1.09551	0.243	10.48	11.41	7.57	20.11±0.23	19.99±0.17	0.85	11.06	1.12	9.27
587731187799753015	326.25107	1.19933	0.204	10.39	0.77	9.82	19.91±0.22	19.24±0.11	1.32	10.12	1.47	8.86
587726877808591211	333.18124	-9.00390	0.247	10.40	12.67	7.40	20.35±0.25	19.98±0.12	0.71	11.08	0.82	...
587726879958302970	338.32794	-7.73724	0.210	10.39	11.18	7.49	19.97±0.23	19.38±0.15	1.09	11.02	0.90	...
587726877811605723	340.03107	-9.63157	0.154	10.42	11.17	7.53	19.14±0.20	19.46±0.14	2.19	10.97	0.54	...
587726877274800314	340.15994	-10.09933	0.084	10.37	8.62	7.70	17.85±0.10	17.72±0.06	3.27	10.55	-0.02	...

Table 1—Continued

SDSS ObjID	RA (deg)	Dec (deg)	Redshift	$\log L_{1530}$ (L_{\odot})	$r_{50,u}$ (kpc)	$\log I_{1530}$ ($L_{\odot} \text{ kpc}^{-2}$)	FUV (mag)	NUV (mag)	A_{1530} (mag)	$\log M_{*}$ (M_{\odot})	$\log \text{SFR}$ ($M_{\odot} \text{ yr}^{-1}$)	$12+\log(\text{O}/\text{H})$
(1)	(2)	(3)	(4)	(5)	(6)	(7)	(8)	(9)	(10)	(11)	(12)	(13)
587730815752667321	340.18524	-10.27453	0.257	10.51	6.55	8.08	20.18±0.29	19.98±0.21	3.29	10.76	1.37	...
587730817365245979	344.72656	-9.34214	0.116	10.50	3.40	8.64	18.30±0.09	17.84±0.04	0.67	9.97	1.15	8.65
587731187808731205	346.76562	1.21978	0.126	10.43	0.71	9.93	18.66±0.02	18.27±0.01	0.65	10.15	0.92	8.82
587731187809059012	347.51736	1.17908	0.207	10.41	6.18	8.03	19.88±0.20	19.75±0.13	2.19	11.10	1.06	9.16
588015508191051903	349.55417	-0.69060	0.252	10.85	2.40	9.29	19.27±0.04	18.82±0.02	0.76	9.92	1.56	8.68
587731186736365813	349.90442	0.22842	0.185	10.74	20.00	7.34	18.79±0.03	19.63±0.03	...	10.85	0.50	...
587731187273892048	351.41345	0.75200	0.277	10.52	1.06	9.67	20.32±0.06	20.20±0.03	0.73	9.31	0.78	8.61
587731187811549347	353.21692	1.23279	0.187	10.33	6.85	7.86	19.84±0.24	20.03±0.18	1.48	10.33	0.64	9.06
587731186737938564	353.46399	0.28075	0.198	10.50	7.96	7.90	19.56±0.19	19.27±0.12	1.17	10.56	1.61	8.96
587731186738266349	354.30264	0.27763	0.212	10.51	8.15	7.89	19.69±0.19	19.60±0.10	2.36	10.37	0.94	8.99
588015509266890925	354.41162	0.05134	0.186	10.31	8.35	7.67	19.87±0.20	20.39±0.15	3.09	10.59	0.45	...
588015510342402184	358.44873	0.90061	0.223	10.48	2.17	9.01	19.89±0.19	20.03±0.14	0.27	9.55	0.53	8.22
588015510342468082	358.57800	0.94167	0.232	10.42	11.38	7.51	20.13±0.22	20.23±0.16	1.07	10.71	1.04	9.07
587727225152733191	358.70636	-10.97845	0.121	10.35	1.89	9.00	18.76±0.12	18.38±0.06	0.74	10.08	0.94	8.62
588015509269053589	359.30862	0.14575	0.262	10.38	7.69	7.81	20.53±0.26	19.56±0.12	2.32	11.01	1.59	8.89

Note. — UVLG sample. Col. (1): SDSS Object ID number. Col. (2): Right Ascension (2000). Col. (3): Declination (2000). Col. (4): Redshift from SDSS pipeline. Col. (5): \log of FUV luminosity (corrected for Galactic extinction). Col. (6): Seeing-corrected half light radius in u -band. Col. (7): \log of FUV surface brightness (corrected for Galactic extinction). Col. (8): FUV magnitude (corrected for Galactic extinction). Col. (9): NUV magnitude (corrected for Galactic extinction). Col. (10): FUV attenuation using the Balmer decrement measured on the SDSS spectra, and the Calzetti (2001) starburst attenuation law. Col. (11): \log of stellar mass determined via SED fitting. Col. (12): \log of extinction-corrected star formation rate determined via SED fitting. Col. (13): Metallicity using the Tremonti et al (2004) method.

Table 2. Comparison of Galaxy Properties

Parameter	Large UVLGs	Compact UVLGs ($I_{1530} > 10^8 L_{\odot} \text{ kpc}^{-2}$)	Supercompact UVLGs ($I_{1530} > 10^9 L_{\odot} \text{ kpc}^{-2}$)	LBGs ^a
Number	110	105 ^b	35 ^b	...
$\log L_{1530} (L_{\odot})$	10.3 to 11.2	10.3 to 11.0	10.3 to 10.9	10.3 to 11.3
$\log I_{1530} (L_{\odot} \text{ kpc}^{-2})$	6.0 to 8.0	8.0 to 10.3	9.0 to 10.3	9 to 10
$\log R_{50,u} (\text{kpc})$	0.9 to 1.6	-0.5 to 0.8	-0.5 to 0.4	0.0 to 0.5
$\log M_* (M_{\odot})$	10.3 to 11.7	9.2 to 11.0	9.0 to 10.7	9.5 to 11.0
A_{1530}	0 to 5	0 to 2.5	0 to 2	0 to 3
$\log \text{SFR} (M_{\odot} \text{ yr}^{-1})$	0 to 1.5	0.2 to 2	0.5 to 2	0.5 to 2.5
$\log \text{SFR}/M_* (\text{yr}^{-1})$	-11 to -9.5	-10.5 to -8	-9.3 to -8	-9 to -8
$\text{FUV}-r$	1.0 to 3.5	0.2 to 2.8	0.2 to 1.7	0.2 to 2.2
$12+\log(\text{O}/\text{H})^c$	8.6 to 9.3	8.5 to 9.2	8.2 to 8.9	7.7 to 8.8
$12+\log(\text{O}/\text{H})^d$	8.4 to 8.9	8.2 to 8.8	8.1 to 8.8	8.2 to 8.6

^aProperties for LBGs are taken from Shapley et al. (2001), Erb et al. (2006a), Papovich et al. (2001), Giavalisco et al (2002), and Ferguson et al. (2004).

^bThe supercompact UVLGs are a subset of the compact UVLGs, *i.e.*, the compact UVLG sample includes the 35 supercompact UVLGs.

^cMetallicity determined using the Tremonti et al (2004) technique.

^dMetallicity determined using the $N2$ technique (see Pettini & Pagel 2004; Erb et al 2006a.)

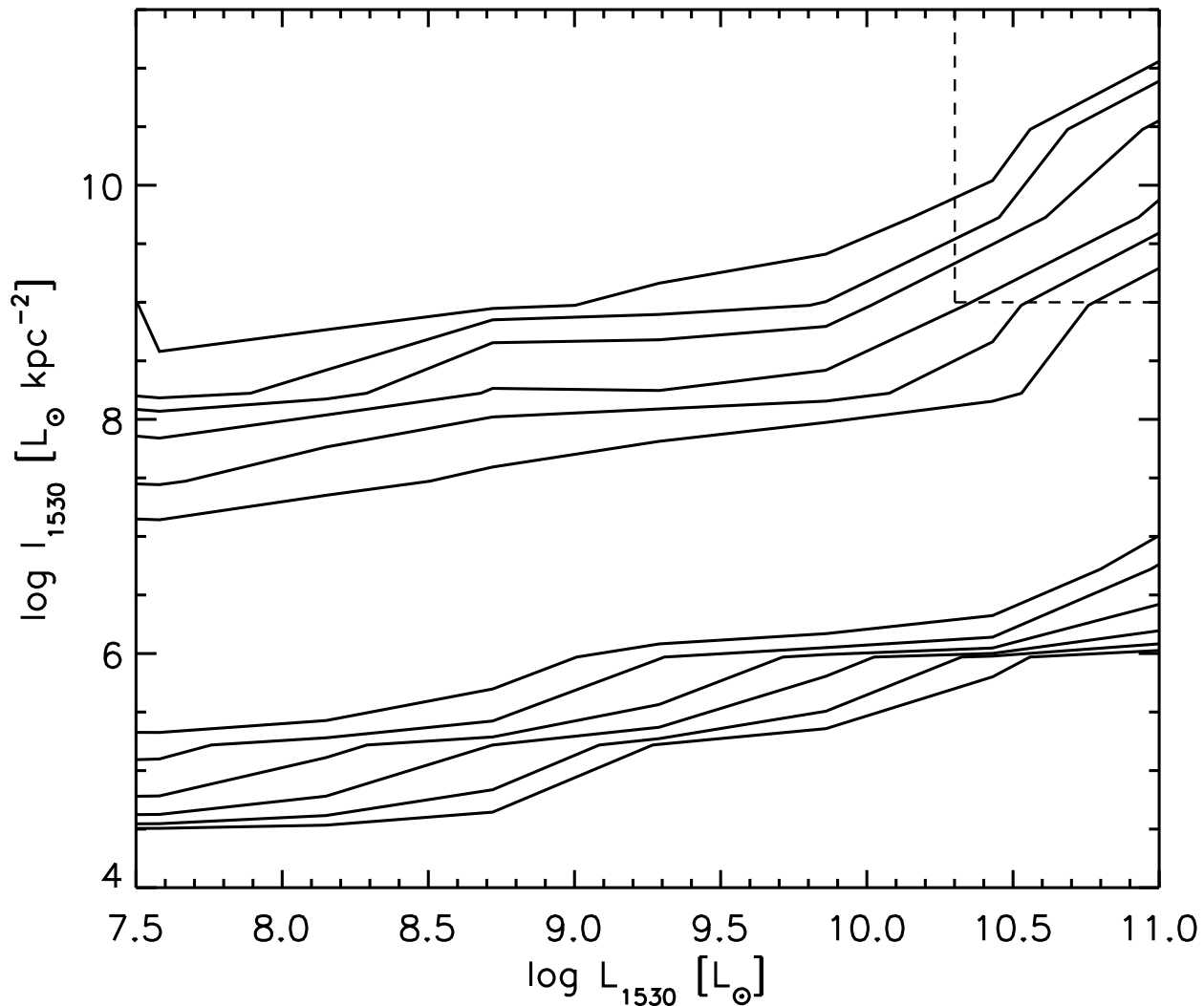


Fig. 1.— Normalized contour plot of the FUV surface brightness versus FUV luminosity for 18463 galaxies in the GR1/DR3 sample with FUV detections. The luminosity bins are normalized to have the same number of galaxies in each bin. Each pair of contours represents a factor of two increase in the enclosed fraction of galaxies in the luminosity bin that have surface brightness in a given range, with the central pair of contours enclosing 84% of the galaxies in the luminosity bin, and the outer pair of contours enclosing 99.5% of the galaxies. FUV luminosity (L_{1530}) is defined as λP_{λ} at 1530 Å (observed wavelength). FUV surface brightness is defined as $I_{1530} = L_{1530}/(2\pi r_{50,u}^2)$, where $r_{50,u}$ is the SDSS u -band half-light radius (corrected for seeing). The data points in this figure have been corrected for Galactic foreground extinction, but not for internal extinction. The dashed line shows the region typically populated by LBGs.

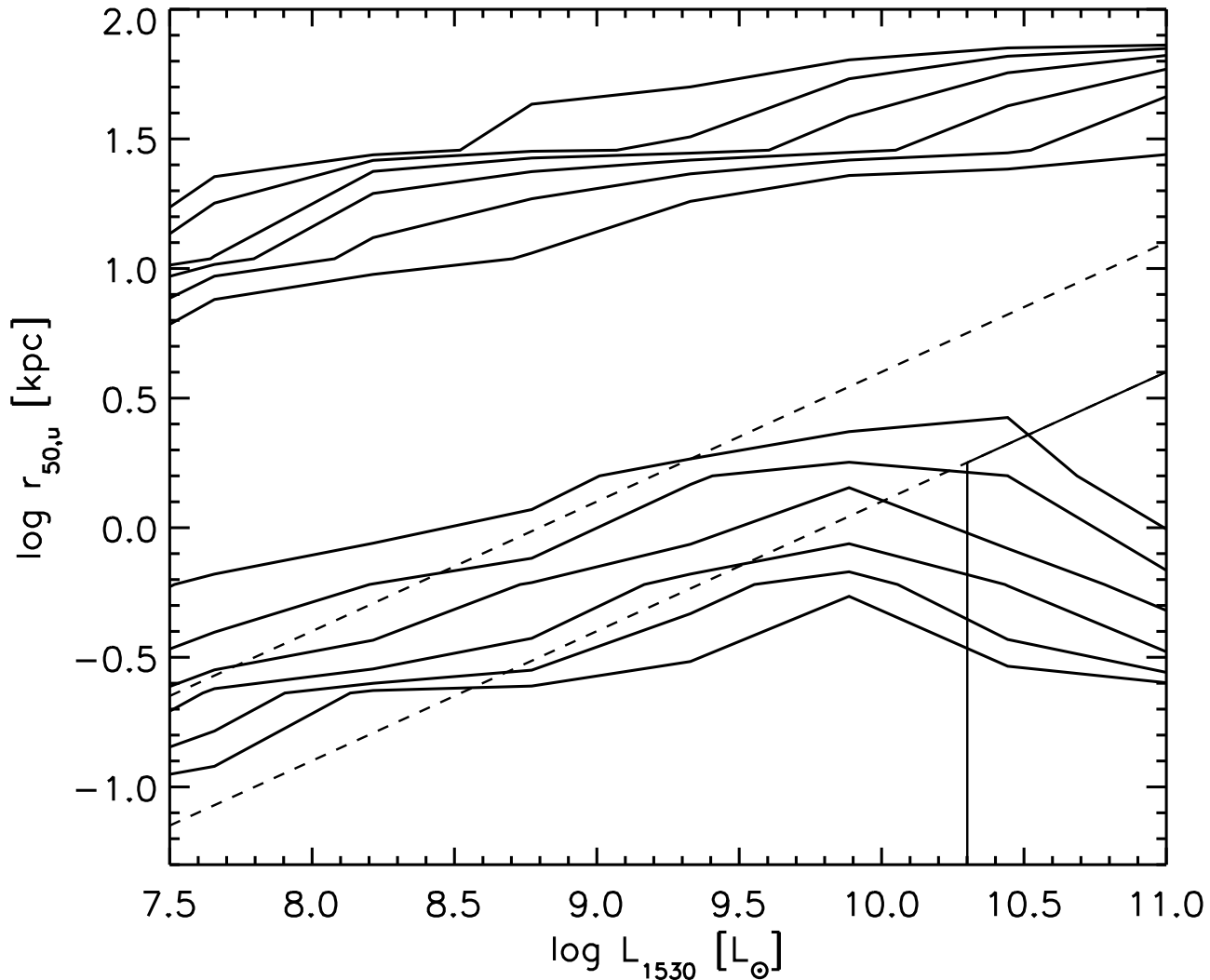


Fig. 2.— Normalized contour plot of the u -band half-light radius versus FUV luminosity for 18463 galaxies in the GR1/DR3 sample that have FUV detections. The luminosity bins are normalized to have the same number of galaxies in each bin. Each pair of contours represents a factor of two increase in the enclosed fraction of galaxies in the luminosity bin that have surface brightness in a given range, with the central pair of contours enclosing 84% of the galaxies in the luminosity bin, and the outer pair of contours enclosing 99.5% of the galaxies. The SDSS u -band half-light radius is derived from an exponential model fit and includes a seeing correction. The dashed lines denote FUV surface brightness levels of $I_{1530} = 10^8 L_{\odot} \text{ kpc}^{-2}$ (upper line) and $I_{1530} = 10^9 L_{\odot} \text{ kpc}^{-2}$ (lower line). The solid line shows the region typically populated by LBGs. The data points in this figure have been corrected for Galactic foreground extinction, but not for internal extinction.

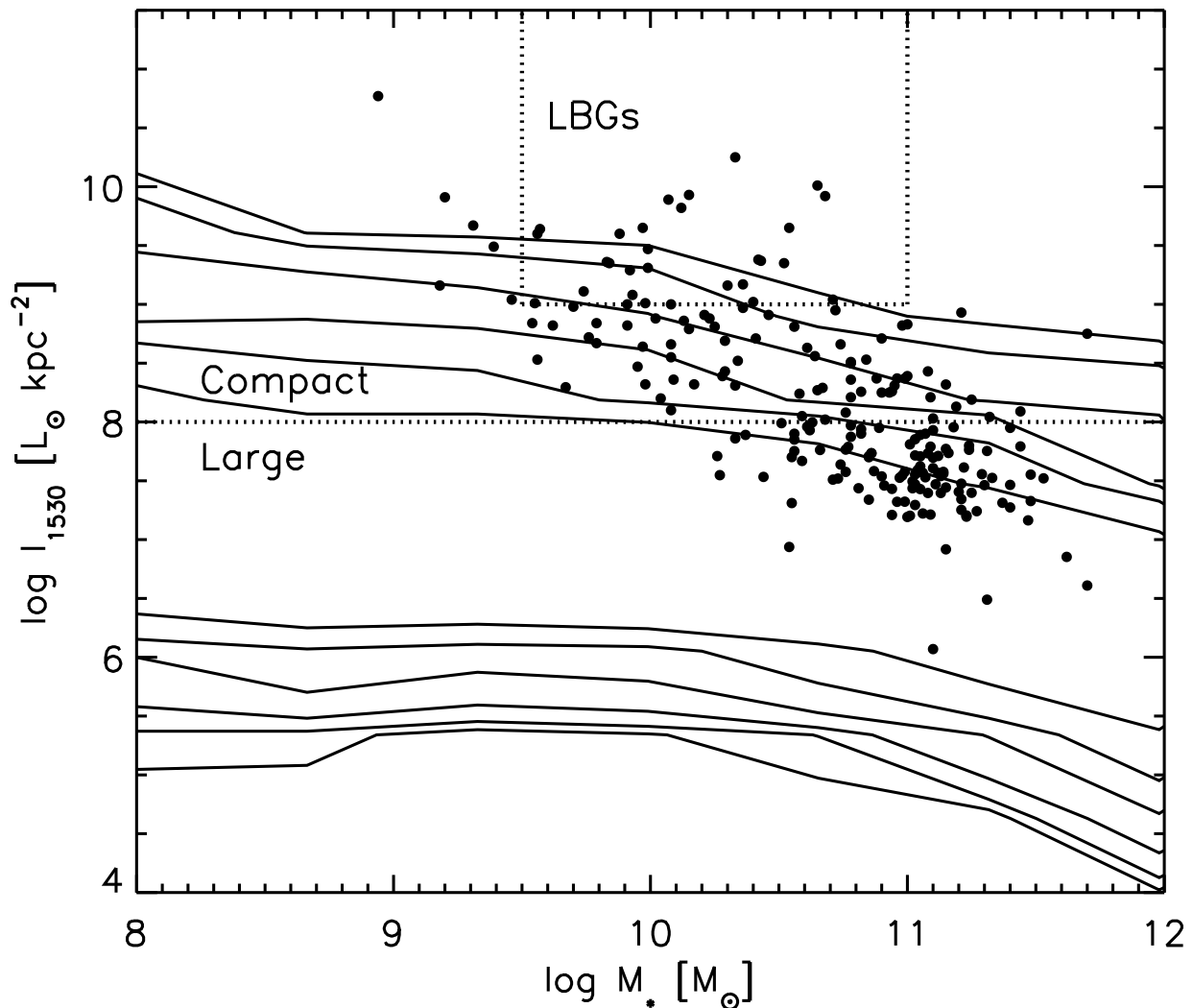


Fig. 3.— Normalized contour plot of the FUV surface brightness versus stellar mass for the 18463 galaxies in the GR1/DR3 sample that have FUV detections. The stellar mass bins are normalized to have the same number of galaxies in each bin. Each pair of contours represents a factor of two increase in the enclosed fraction of galaxies in the mass bin that have surface brightness in a given range, with the central pair of contours enclosing 84% of the galaxies in the mass bin, and the outer pair of contours enclosing 99.5% of the galaxies. The individual galaxies in the UVLG sample are shown as points in the plot. The boundaries of mass and surface brightness for typical LBGs are also shown in the figure, as is the boundary between large and compact UVLGs.

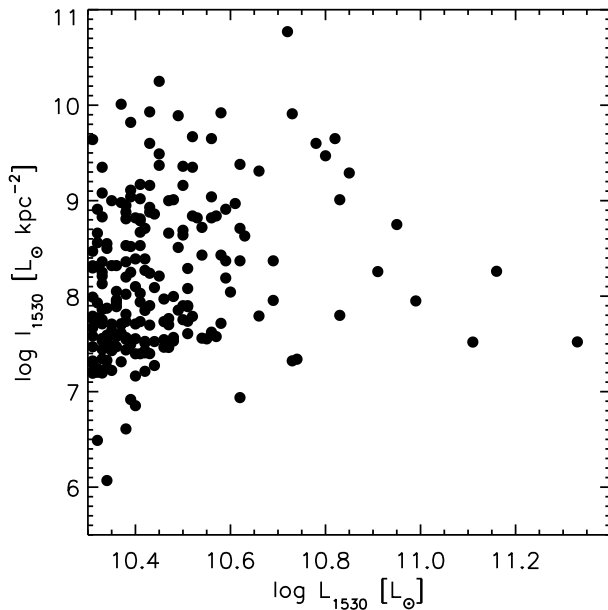


Fig. 4.— FUV surface brightness versus FUV luminosity for 215 UVLGs in the GR1/DR3 sample. FUV luminosity (L_{1530}) is defined as λP_{λ} at 1530 \AA . FUV surface brightness is defined as $I_{1530} = L_{1530}/(2\pi r_{50,u}^2)$, where $r_{50,u}$ is the SDSS u -band half-light radius.

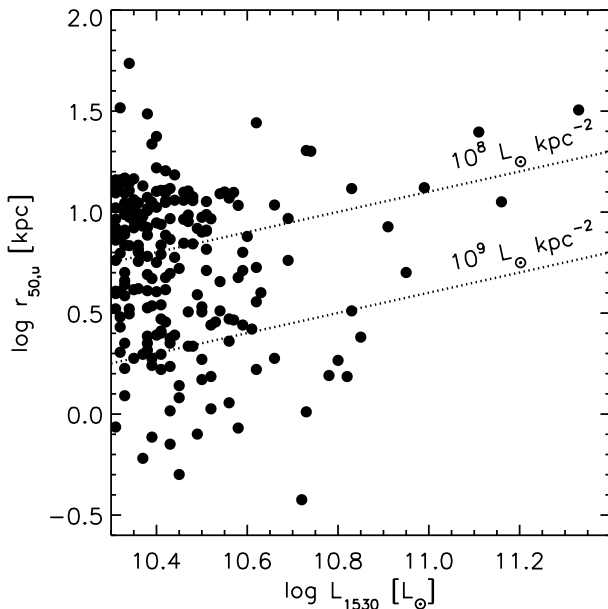


Fig. 5.— Half-light radius in the SDSS u -band versus FUV luminosity for 215 UVLGs in the GR1/DR3 sample. FUV luminosity (L_{1530}) is defined as λP_{λ} at 1530 \AA . The upper dotted line shows a constant surface brightness of $10^8 L_{\odot} \text{ kpc}^{-2}$, which is our chosen boundary between large and compact UVLGs, and the lower dotted line shows $I_{1530} = 10^9 L_{\odot} \text{ kpc}^{-2}$, which is the lower boundary of values seen in typical LBGs at $z = 3$ (Giavalisco 2002).

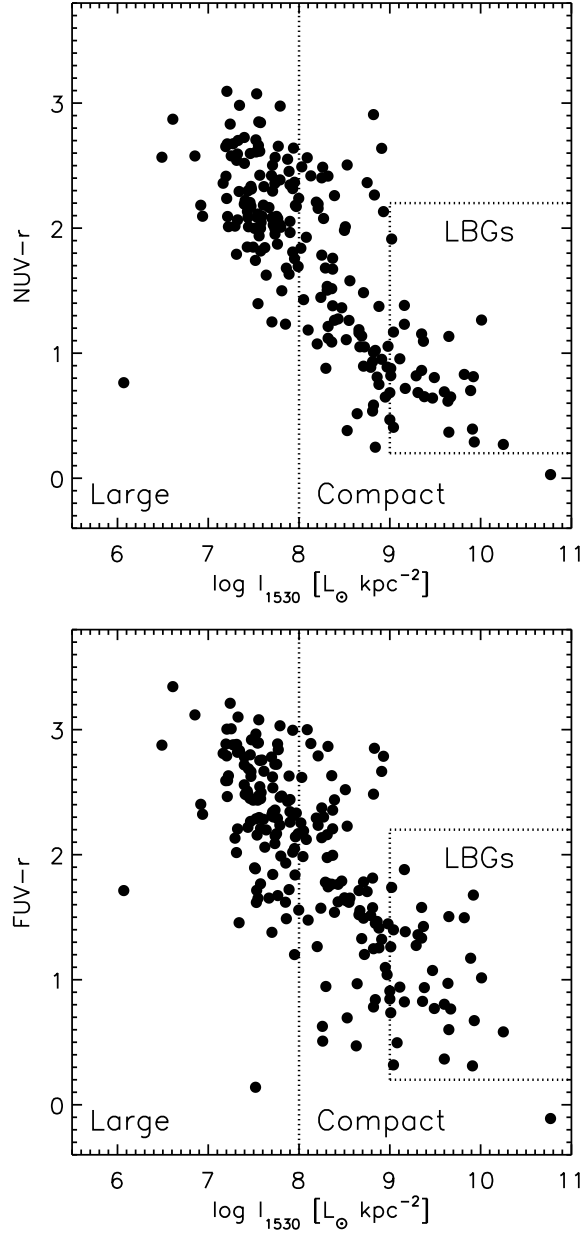


Fig. 6.— *top*: FUV- r color versus FUV surface brightness for 215 UVLGs in the GR1/DR3 sample. FUV surface brightness is defined as $I_{1530} = L_{1530}/(2\pi r_{50,u}^2)$, where $r_{50,u}$ is the SDSS u -band half-light radius. The dotted line shows the boundaries of FUV- r color and surface brightness for typical LBGs. *bottom*: NUV- r color versus FUV surface brightness for 215 UVLGs in the GR1/DR3 sample.

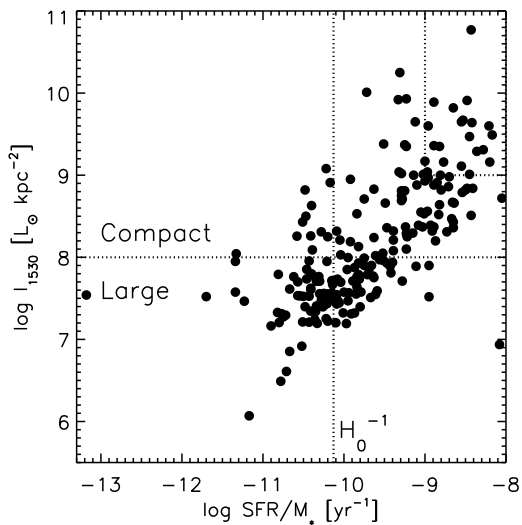


Fig. 7.— FUV surface brightness versus specific star formation rate (extinction-corrected star formation rate divided by stellar mass) for 215 UVLGs in the GR1/DR3 sample. The stellar mass and star formation rate were determined via SED fitting. FUV surface brightness is defined as $I_{1530} = L_{1530}/(2\pi r_{50,u}^2)$, where $r_{50,u}$ is the SDSS u -band half-light radius. The boundaries of specific SFR and surface brightness for typical LBGs are marked (the small region in the upper right outlined by a dotted line), as is the value of the Hubble time for our chosen cosmology.

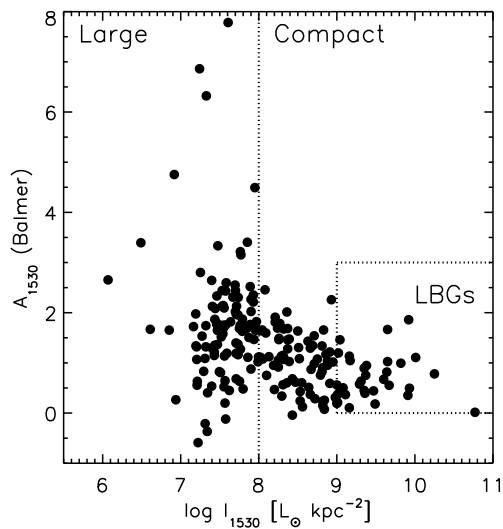


Fig. 8.— Attenuation of the FUV continuum versus FUV surface brightness for the 210 UVLGs in the GR1/DR3 sample with good line flux measurements. FUV surface brightness is defined as $I_{1530} = L_{1530}/(2\pi r_{50,u}^2)$, where $r_{50,u}$ is the SDSS u -band half-light radius. The FUV attenuation was determined using the Balmer decrement in the SDSS spectra and the Calzetti (2001) starburst attenuation law, in which $E(B - V)_{\text{continuum}} = 0.44E(B - V)_{\text{lines}}$. Four large UVLGs are not shown because they have no emission lines in the SDSS fiber spectra, and one supercompact UVLG has an apparent anomaly in the spectrum near $H\alpha$. The dotted line shows the boundaries of FUV attenuation and surface brightness for typical LBGs.

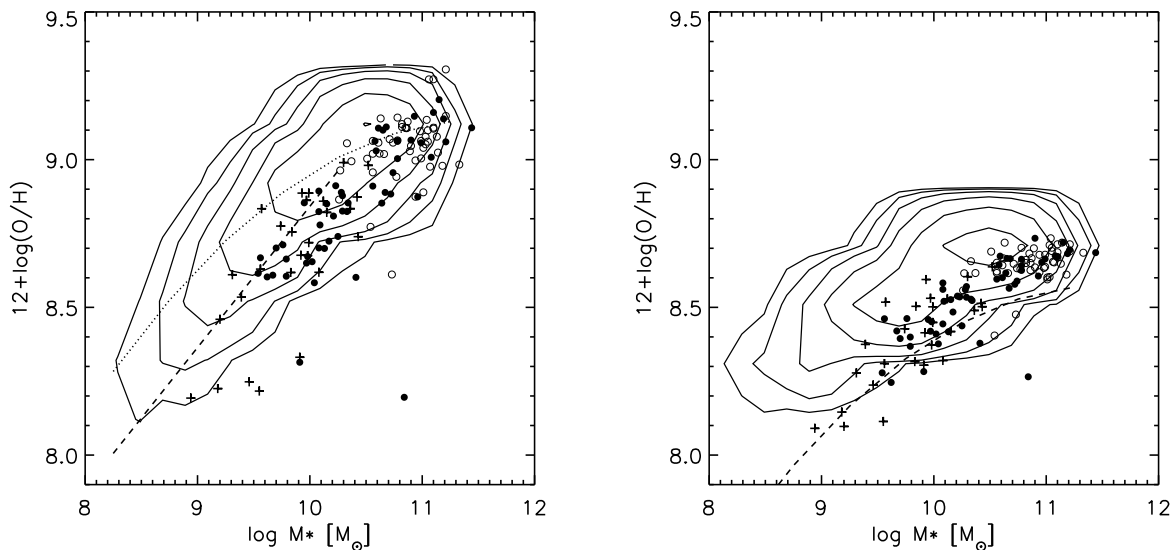


Fig. 9.— *Left*: The dependence of metallicity upon stellar mass. The O/H estimates were derived from the SDSS spectra using the technique described in Tremonti et al. (2004), and the stellar mass was determined via SED fitting (Salim et al. 2005). The contours represent 10002 galaxies in the GR1/DR3 sample which have good metallicity measurements. The individual galaxies in the UVLG sample are shown as points in the plot. Open circles are UVLGs with $I_{1530} < 10^8 L_{\odot} \text{ kpc}^{-2}$ (large UVLGs), and filled circles are UVLGs with $10^8 L_{\odot} \text{ kpc}^{-2} < I_{1530} < 10^9 L_{\odot} \text{ kpc}^{-2}$ (compact UVLGs). UVLGs with $I_{1530} > 10^9 L_{\odot} \text{ kpc}^{-2}$ (supercompact UVLGs) are denoted as crosses. The dotted line is the best fit to the Tremonti et al. (2004) sample, and the dashed line is the fit from Savaglio et al. (2005). *Right*: Same as the left panel, but using the $N2$ method as calibrated by Pettini & Pagel (2004). The dashed line is from Erb et al. (2006), which is the Tremonti et al. (2004) fit displaced downward by 0.56 dex.

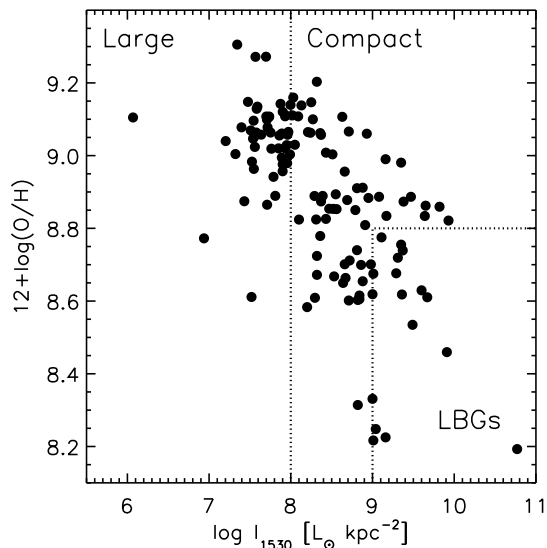


Fig. 10.— FUV surface brightness versus metallicity for 129 UVLGs in the GR1/DR3 sample which have good metallicity measurements (galaxies with an AGN contribution to their spectra were removed). FUV surface brightness is defined as $I_{1530} = L_{1530}/(2\pi r_{50,u}^2)$, where $r_{50,u}$ is the SDSS u -band half-light radius. The O/H estimate is derived from the SDSS spectra (Tremonti et al. 2004). The dotted line shows the boundaries of $12+\log(\text{O}/\text{H})$ and surface brightness for typical LBGs.

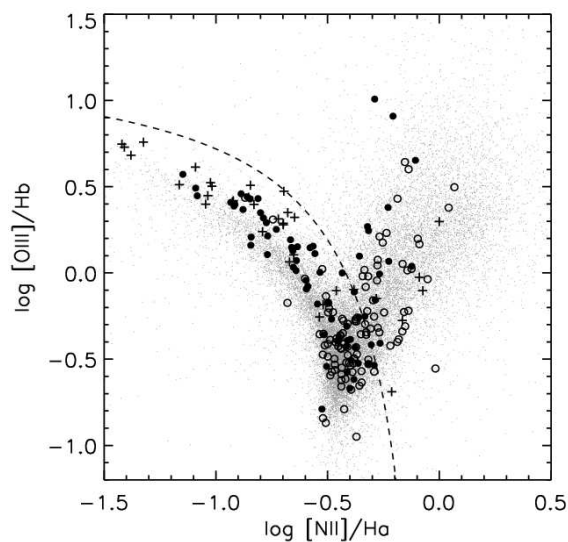


Fig. 11.— A BPT diagram (Baldwin et al. 1981) for the 23400 galaxies with good line flux measurements in the DR3/GR1 sample. The dashed curve shows the demarcation between starburst and AGN defined by Kauffmann et al. (2003c). The large circles and crosses are UVLGs. There are 106 large UVLGs (open circles), 70 compact UVLGs (filled circles), and 34 supercompact UVLGs (crosses) shown in this plot. Four large UVLGs are not shown because have no emission lines in the SDSS fiber spectra, and one supercompact UVLG has an apparent anomaly in the spectrum near $\text{H}\alpha$.

